Hybrid Train Power with Diesel Locomotive and Slug Car–Based Flywheels for NOx and Fuel Reduction

Zhiyang Wang[1]; Alan Palazzolo[2]; and Junyoung Park[3]

Abstract: An energy-storage flywheel consists of a large inertia wheel sharing a common shaft with a motor generator (MG) set and with magnetic bearings to support the entire rotating assembly. Flywheels mounted on a special slug car are charged from the local utility grid and from regenerative-braking events. Usage of these power sources reduces fuel consumption and the related NOx emission by the locomotive-mounted Diesel generator sets (DGS). The flywheel-supplied power can replace the DGS-supplied power in one or more of the eight fixed power settings (notches), plus idle and reverse, which are common to most locomotives either for line-haul or switchyard service. The slug cars have separate traction motors to be driven by the flywheel systems so that the flywheel power and DGS power are electrically and physically decoupled. A system model is presented that includes the train dynamics coupled with the electromechanical models for the flywheels and traction motors. The modified Davis equation is employed in the train model to account for windage and other losses. A novel, feedback-based flux-weakening control of the flywheel's motor generator current-torque and speed-back electromotive force (emf) gain is employed to increase the charge capacity, depth of discharge, and regenerative-braking efficiency for the flywheels. The simulation results show significant cost- and emissions-reduction potential for the proposed hybrid DGS–flywheel locomotive power system in line-haul and switcher service. **DOI: 10.1061/(ASCE)EY.1943-7897.0000081.** © *2012 American Society of Civil Engineers.*

CE Database subject headings: Emissions; Environmental issues; Energy storage; Rail transportation; Fuels.

Author keywords: Green technology; Emissions reduction; Energy storage; Railroad; Locomotive; Flywheel; Smart technology; Regenerative breaking; Energy harvesting; All electric; Hybrid power.

Introduction and Background

Energy storage is an important enabling technology for developing clean and renewable energy resources and for energy-harvesting processes. The objective of this manuscript is to present a novel approach for the usage of energy-storage flywheels for harvesting and reusing braking energy and for providing a portable power source that derives energy from the electrical grid. Grid-generated power is obtained with far less NOx emissions than are produced by the portable Diesel engine generator sets on locomotives.

A flywheel-powered locomotive was developed by Maschinenfabrik Oerlikon of Switzerland (1958) for the National Coal Board (NCB) at Seaton Delaval to be a fire- and emission-free candidate for underground applications. The four-wheel, 150-kw locomotive was powered solely by two flywheels. In 1979, the U.S. Federal Railroad Administration (FRA) sponsored research on a switcher locomotive powered by flywheel energy storage (AiResearch Manufacturing Company of California 1979). The 4.5-kW · h flywheel model employed for the investigation had a calculated parasitic loss of 7.22 kW attributable to the use of roller bearings and a planetary gear train between the flywheel and MG. This flywheel design would dissipate 100% of its energy within 38 min. In comparison, modern flywheels are supported on magnetic bearings, have motor generators that are integral with the flywheel shaft, and have highly efficient power-conversion systems, yielding energy losses between 5% and 10% over a 24-h period, while operating in an idle mode. The University of Texas at Austin Center for Electromechanics (UT-CEM) developed an advanced locomotive propulsion system (ALPS) flywheel with a design energy storage of 130 kW · h and peak power of 2 MW for hybrid locomotive power as part of the next-generation high-speed rail program (Thelen et al. 2003; Caprio et al. 2004). The hybrid power system consisted of a gas turbine–driven generator, along with a flywheel to supply supplemental power from the turbine while climbing grades or for other peak power demands. This enabled optimization of the 3,730-kw gas turbine performance design for a steady operating point without the constraint of peak power demand. Research has also been conducted on incorporation of flywheels in passenger cars and buses for brake-energy harvesting and for supplemental peak power (Brockbank and Greenwood 2009; Hawkins et al. 2003; Huang and Wang 2007). The National Aeronautics and Space Administration (NASA) (Kenny et al. 2005) has built a series of advanced energy-storage flywheels for potential satellite applications. The usage of high-speed flywheels for integrated power and attitude control system (IPACS) on satellites (Park et al. 2008) has also been investigated.

The use of a hybrid train power system is proposed, consisting of contributions from a bank of flywheels that provide propulsion power for a slug car, and Diesel generator sets, which provide propulsion power for the locomotives. A conventionally powered slug car has traction motors (TMs) that derive their power from the Diesel generator sets on the locomotives, through electrical cabling, and are used to increase traction force by dividing it between the locomotive and the slug car. In the proposed approach, the slug car

[1]Ph.D. Candidate, Vibration Control and Electromechanics Laboratory, Dept. of Mechanical Engineering, MS 3123, Texas A&M Univ., College Station, TX 77843-3123.

[2]Professor, Vibration Control and Electromechanics Laboratory, Dept. of Mechanical Engineering, MS 3123, Texas A&M Univ., College Station, TX 77843-3123 (corresponding author). E-mail: a-palazzolo@tamu.edu

[3]Samsung Corp., Seoul, South Korea.

Note. This manuscript was submitted on July 1, 2011; approved on April 2, 2012; published online on April 11, 2012. Discussion period open until May 1, 2013; separate discussions must be submitted for individual papers. This paper is part of the ***Journal of Energy Engineering***, Vol. 138, No. 4, December 1, 2012. © ASCE, ISSN 0733-9402/2012/4-215-236/$25.00.

traction motors are powered by, and deliver regenerative-braking power to, a bank of flywheels located on the slug car. An alternative approach is to carry the flywheels in a freight car with a cable connection to the locomotive traction motors.

The effectiveness of the proposed system is evaluated by simulation utilizing average power duty cycles for line-haul and switcher service, published by the EPA (Sierra Research Inc. 2004). In the report, the main generator in a locomotive is driven by a Diesel engine, which consumes on average 220 L of Diesel fuel per hour in line-haul service and 76 L/h in switch-yard service. The generated electricity powers a set of TMs that exert torques on the locomotive wheels through geared transmissions located between the TMs and the locomotive's wheels. The wheels then propel the train forward or in reverse. The TMs may also act as traction generators (TGs), in which case the TG shafts exert braking torques on the train wheels. This torque brakes the train, while the electric currents that are generated in the TGs are dissipated as waste heat in resistor banks. The emission measurements from locomotives are made at each notch setting, and the average emissions for the locomotive are computed from an assumed duty cycle (representing normal locomotive operation in the field). The average NOx emissions for tier-2 class Diesel engine locomotives are approximately 12.7 kg/h for line-haul and 3.5 kg/h for switchyard service. As a reference, 24-h/day, 365-days/year service yields NOx emissions of 122 t/year for line-haul and 33.8 t/year for switchyard service. The present paper investigates the feasibility of reducing train NOx emissions by utilizing a portable electrical energy source (PEES) such as an onboard bank of flywheels that are charged from the (low NOx) local utility grid at train stations, from the energy produced by braking the train (i.e., regenerative braking), or from an onboard Diesel engine that runs more efficiently. The PEES will drive TMs on their corresponding slug cars, which are separate from Diesel locomotive ones, and supplement or replace driving power produced by the Diesel engines.

The U.S. annual NOx emission rate for grid electricity as of 2007 is 0.8 kg/MW · h, as released in the EPA's eGRID2010 files (EPA 2010). The NOx emissions for average Diesel engine notches can vary between 8.93 and 16.58 kg/MW · h, according to EPA line-haul and switcher data (Sierra Research Inc. 2004), which is up to 20 times that of grid electricity. The grid electricity cost paid by the railroad is approximately US 11.17 = kW · h, as released by the U.S. Energy Information Administration (2010). At a Diesel price of US 0.925 = L (US 3.5 = gal:), the Diesel unit energy price varies between US 0.221 = kW · h and US 0.916 = kW · h depending on the different power-level efficiencies derived from EPA's report (Sierra Research Inc. 2004). The Diesel fuel cost is approximately 2–8 times the cost of grid electricity, on an equivalent energy basis. In fairness to Diesel power, its upper cost limit corresponds to very low power level, which consumes a relatively small amount of fuel. These comparisons support the usage of PEES to reduce emissions and operating costs.

Flywheel energy-storage systems (FESS) have no chemical battery disposal issues, are more robust for temperature extremes, are similar to batteries in energy density, and can operate with lower depths of discharge and longer life than batteries (Wilson and Fausz 2006). This is the motivation for the use of flywheels, over batteries, in the proposed approach. The three primary components of a flywheel are a rotating inertia wheel that stores kinetic energy, an MG that provides power conversion between electrical and mechanical (kinetic) forms, and a magnetic suspension (bearing) system that supports the weight of the spinning flywheel with minimal drag. The flywheel rotating assembly is typically supported by a five-axis magnetic bearing system that reacts to the flywheel loads. Patented technology developed by Palazzolo et al. ["System and method for controlling suspension using a magnetic field," U.S. Patent No. 6,323,614B1 (2001); "Fault tolerant homopolar magnetic bearings," U.S. Patent No. 7,429,811 (2008)] improves the fault tolerance of the magnetic bearings and the stability of the magnetically levitated, spinning flywheels. The rotating assembly is housed in a vacuum vessel to minimize windage losses. The flywheel MG receives electrical energy from the utility grid or from the TGs during regenerative braking to spin up the flywheel increasing its rotational kinetic energy. The flywheel MG converts the stored rotational kinetic energy of the flywheel into electrical energy to power the traction motors that propel the train.

Fig. 1 depicts the proposed system structure, which contains the following:

- Diesel locomotives, which have alternating current/direct current (ac/dc) traction motors.
- Slug cars, which have their own dc traction motors physically separated from traction motors on Diesel locomotives. The slug cars do not have Diesel generators and are often filled with dummy weight load (concrete) to increase their traction.
- Flywheel assemblies, which replace the dummy weight on slug cars. They are used to collect regenerative-braking energy and provide propulsion energy when needed.

Modeling

Fig. 2 shows a functional diagram of the proposed hybrid power train using Diesel locomotive and slug car—based flywheel power sources. The flywheels power the traction motors on the slug car and receive power from them during regenerative braking. This approach decouples the electrical systems between the flywheel-powered slug cars and the Diesel engine—powered locomotive. The slug car traction motors act as generators during braking to supply the emf for charging the flywheels, instead of for driving current through resistor banks to dissipate the train's kinetic energy as waste heat, as is presently done on conventional locomotives.

Fig. 3 shows an example Sankey-type power-flow diagram for the proposed system.

The authors of this study employ a simplified dynamics model of the train to highlight the central theme of hybrid power. The

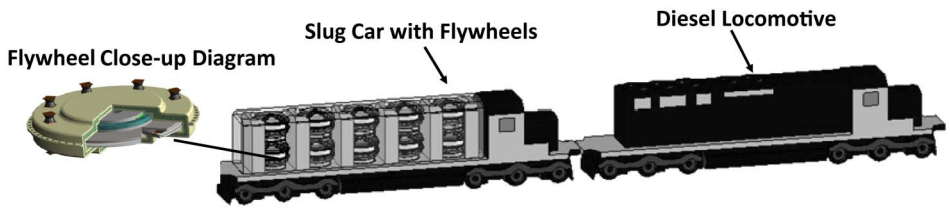

Fig. 1. Train hybrid power source: locomotive and flywheel slug car

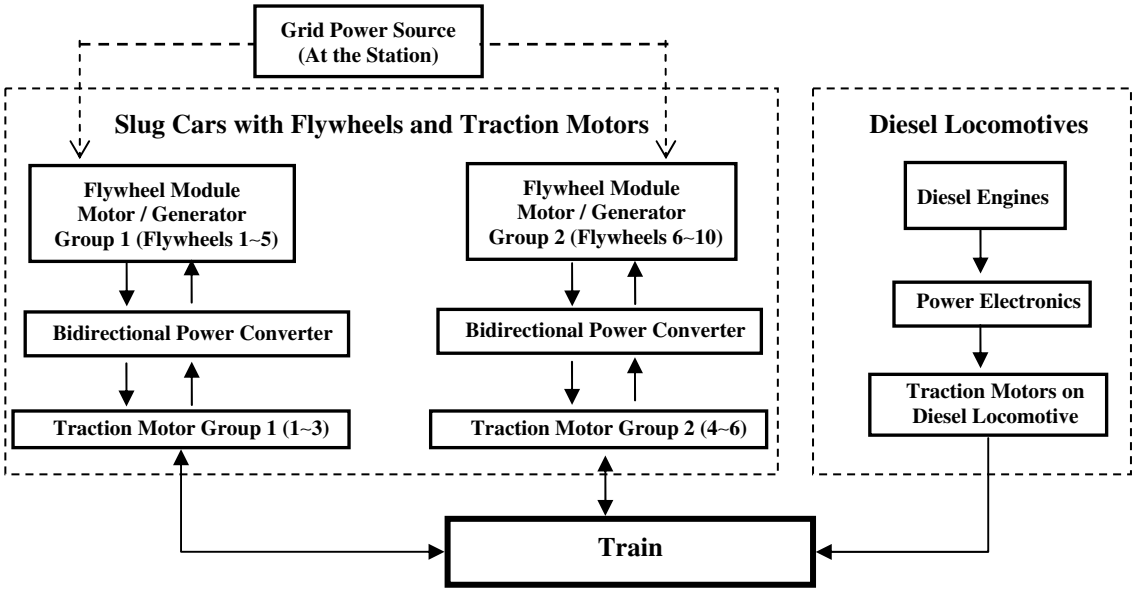

Fig. 2. Train power diagram for hybrid Diesel locomotive–flywheel slug car approach

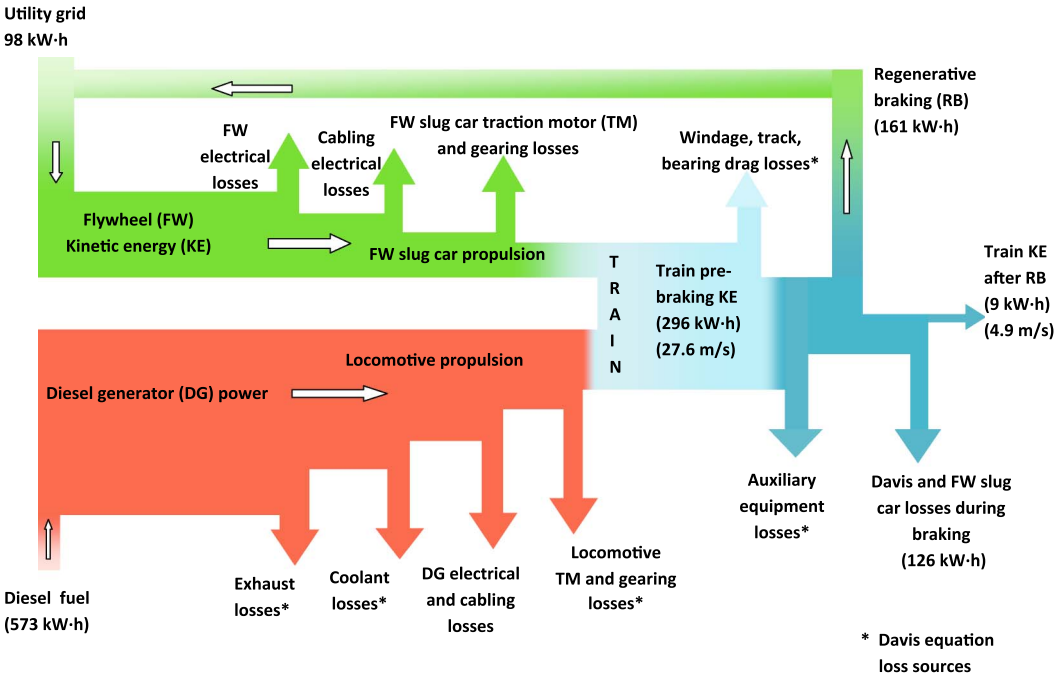

Fig. 3. System energy flow—Sankey diagram for 1 h of EPA average line haul service; regenerative-braking recovered energy may be increased up to more than 200 kW · h with higher K_{tm}

greater detail of higher fidelity train models, such as car pitch and heave, independent bogey motion, and so forth, is intentionally omitted. Consider the following dynamics model of a train with locomotives and a flywheel slug car as in Fig. 4.

There are two general classes of locomotive Diesel engine drive alternators: ac and dc. An ac locomotive Diesel engine drive alternator produces variable-frequency ac, which is rectified to dc, passed on a dc bus to insulated gate bipolar transistor (IGBT) switches, which form a synthetic ac waveform (pulse width modulation) that goes to ac traction motors. A dc locomotive engine drive alternator produces variable-frequency ac (oldest units, dc generator), which is rectified to dc and goes to dc traction motors. The majority of line-haul (over-the-road) locomotives, 3,208 or 3282-kw, delivered to North American railroads over the past decade have ac traction motors. However, there are thousands of older dc locomotives that are still in service and likely will be for many years. A major Canadian railroad remains as a dc-only railroad for line-haul acquisitions because their route structure does not require the higher tractive effort of ac technology. The trans-Canada route is only 0.4% (0.122 m of rise for every 30.5 m of travel). In addition, to the best of the authors' knowledge, there are no switching locomotives available, nor have any been built, using ac motors in North America. The electrical system model presented in this manuscript is most similar to the dc approach described previously.

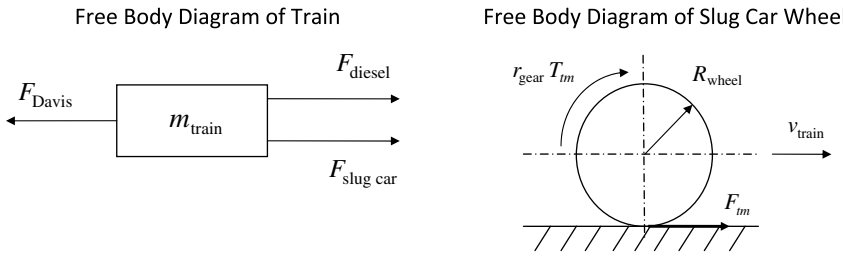

Fig. 4. Train dynamics model

It assumes that the traction motors and flywheel motor generators are dc. The flywheels drive, and are driven by (in regenerative braking), traction motors that are located on the same slug car. This electrical system model is totally uncoupled from the electrical system of the locomotives and their traction motors, which may be dc or ac. A model that includes a complete ac flywheel—traction motor system isolated on its own slug car(s), or coupled with the locomotive electrical system, is planned for future work in a separate manuscript.

A dc electrical system model is employed, in which the flywheel motors supply and recover power to and from the slug car traction motors. Flywheels are available in a wide variety of sizes, weights, powers, and energy-storage levels. For illustration purposes, it is assumed that the slug car has six traction motors and 10 flywheels. Furthermore, it is assumed that there are two groups, each consisting of five flywheels connected in parallel and three traction motors connected in series, as shown in Fig. 5. The cable resistances account for much of the power loss between the source and the load in the system, in which the traction motors and flywheel motors reverse roles as source and load in propulsion and regenerative-braking service. For the sake of illustration, it was assumed that the traction motor and brake bank resistance are in place on the slug car before installing the flywheels, that the wiring harness between the flywheel system and the traction motors and between the flywheel system and braking resistance follow similar length paths, and that their currents are similar so that their wire gauge should be similar. These support the reasonableness of the equal resistance (two R_{cable} symbols in Fig. 5 assumption).

The symbols L_{fw}, R_{fw}, and V_{fw} in Fig. 5 are the single flywheel module inductance, resistance, and voltage, respectively; and L_{tm}, R_{tm}, and V_{tm} are the total inductance, resistance, and voltage of three traction motors connected in series. The flywheels are located on a slug car and only connected to its traction motors, which explains why the locomotive's electrical system is not included in Fig. 5. The cable resistance between components is assumed to be R_{cable}.

The dynamic model of the train can be written as

$$m_{\text{train}}\frac{dv_{\text{train}}}{dt} = F_{\text{train}} = F_{\text{drive}} - F_{\text{davis}} \tag{1}$$

$$F_{tm} = \frac{r_{\text{gear}}T_{tm}}{R_{\text{wheel}}} = r_{\text{gear}}\frac{P_{tm}}{\omega_{tm}}\frac{1}{R_{\text{wheel}}} = \frac{P_{tm}}{v_{\text{train}}} \tag{2}$$

$$F_{\text{diesel}} = \eta_{\text{diesel}}\frac{P_{\text{diesel}}}{v_{\text{train}}} \tag{3}$$

$$F_{\text{drive}} = \begin{cases} F_{\text{diesel}} + F_{\text{slug car}} = F_{\text{diesel}} + n_{tm}F_{tm} = \eta_{\text{diesel}}\frac{P_{\text{diesel}}}{v_{\text{train}}} - \frac{n_{tm}r_{\text{gear}}K_{tm}i_{tm}}{R_{\text{wheel}}} & (F_{\text{drive}} \geq 0, \text{Propulsion}) \\ F_{\text{slug car}} = n_{tm}F_{tm} = -\frac{n_{tm}r_{\text{gear}}K_{tm}i_{tm}}{R_{\text{wheel}}} & (F_{\text{drive}} < 0, \text{Braking}) \end{cases} \tag{4}$$

where m_{train} = train total mass including the flywheel slug car; v_{train} = train velocity; F_{train} = total force acting on the train; F_{drive} = train driving (propulsion) force; F_{diesel} = driving forces generated by the Diesel locomotives; η_{diesel} = Diesel engine power efficiency; $F_{\text{slug car}}$ = driving forces generated by the flywheel slug car; F_{tm} = force exerted on the track by a single traction motor of the slug car; F_{Davis} = train resistance force from the modified Davis equation; r_{gear} = gear ratio between a traction motor and its wheels; T_{tm} = slug car traction motor torque; R_{wheel} = slug car wheel radius; P_{tm} = slug car traction motor power; ω_{tm} = traction motor angular velocity; n_{tm} = number of traction motors on the slug car; P_{diesel} = Diesel locomotive power; K_{tm} = slug car traction motor torque constant; and i_{tm} = slug car traction motor current, which is positive during braking phase and negative during propulsion phase. F_{Davis} represents the modified Davis drag force (MDF) (William 1982), which is a conservative, empirically based formula that accounts for air resistance, track and rolling resistance, bearing resistance, windage and friction in the traction motors, lighting, and so forth. This drag force varies with train and car weight, velocity, and other factors. In its standard form, the modified Davies formula is converted into SI units and given as

$$R_u = \left(0.6 + \frac{20 \times 907}{w} + \frac{0.01v}{1.6} + \frac{907K_{\text{air}}v^2}{2.56wn}\right) \times 0.004904 \tag{5}$$

where R_u = resistance force in N/kg; w-car mass per axle (in kg); n = number of axles per car; v = speed in km/h; and K_{air} is the air drag coefficient. Therefore

$$F_{\text{davis}} = m_{\text{train}} \times R_u = A + Bv + Cv^2 \text{ (Newton)} \tag{6}$$

where

$$A = \left(2.942 \times 10^{-3} + \frac{88.96}{w}\right)m_{\text{train}} \tag{7}$$

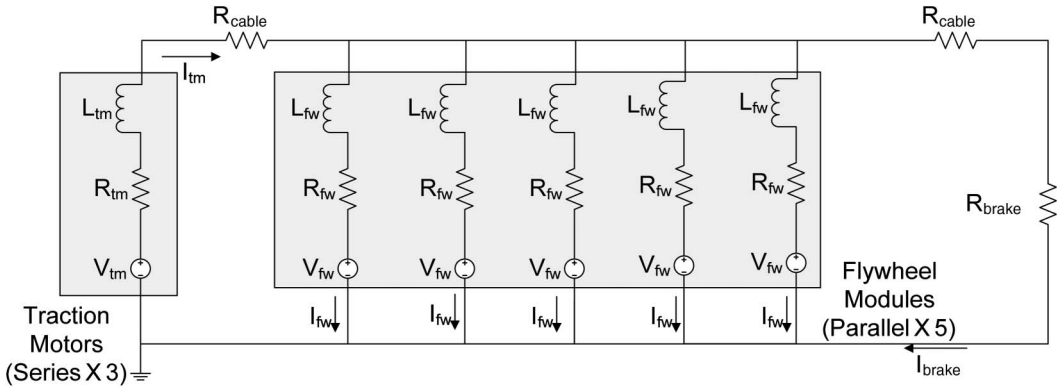

Fig. 5. Equivalent circuit model for one group of three traction motors and five flywheels on a slug car

$$B = 3.065 \times 10^{-5} v m_{\text{train}} \tag{8}$$

$$C = 1.7375 \frac{K_{\text{air}} m_{\text{train}}}{wn} \tag{9}$$

The flywheel rotational (spin) motion is governed by

$$I_{Pfw}\dot{\omega}_{fw} = T_{fw} = K_{fw} i_{fw} - C_{fw}\omega_{fw} \tag{10}$$

where I_{Pfw} = polar moment of inertia of the flywheel; T_{fw} = torque on flywheel; ω_{fw} = flywheel rotational speed; K_{fw} = flywheel motor torque constant; i_{fw} = flywheel motor current; and C_{fw} = flywheel drag torque coefficient attributable to eddy current drag.

Application of Kirchhoff's laws yields

$$i_{tm} = 5 i_{fw} + i_{\text{BRAKE}} \tag{11}$$

$$\begin{bmatrix} (5L_{tm} + L_{fw}) & L_{tm} \\ L_{fw} & 0 \end{bmatrix} \begin{bmatrix} \frac{d}{dt} i_{fw} \\ \frac{d}{dt} i_{\text{brake}} \end{bmatrix} = \begin{bmatrix} -(5R_{tm} + 5R_{\text{cable}} + R_{fw}) & -(R_{tm} + R_{\text{cable}}) \\ -R_{fw} & (R_{\text{cable}} + R_{\text{brake}}) \end{bmatrix} \begin{bmatrix} i_{fw} \\ i_{\text{brake}} \end{bmatrix} + \begin{bmatrix} V_{tm} - V_{fw} \\ -V_{fw} \end{bmatrix} \tag{12}$$

where R_{brake} = electrical resistance of the slug car's bank of braking resistors; and R_{cable} = cable electrical resistance. The resistor bank would only be used if the braking was required and the flywheels were fully charged.

The torque developed by a single traction motor is

$$T_{tm} = -K_{tm} i_{tm} \tag{13}$$

The three traction motors are connected in series, which yields

$$V_{tm} = 3 K_{tm} \omega_{tm} \tag{14}$$

The voltage across an individual flywheel is given by

$$V_{fw} = K_{fw} \omega_{fw} \tag{15}$$

A traction feedback control system is not included in this simplified model to concentrate on hybrid power. The maximum adhesion, which is defined as total traction motor force divided by slug car weight, in the numerical examples presented is 0.19 and appears during the start of braking. As indicated by William (1982), an adhesion value of 0.25 is often assumed as an upper limit for nonslip operation, and with clean and dry rail, the upper limit is 0.3. So this value (0.19) is consistent with a nonslip condition (rolling contact) for the wheels, which justifies exclusion of a traction control component in the present model. The simulations presented in this paper utilized the following limits to replicate typical operating limits encountered in actual locomotive systems:

- Motor gain: $0 < K_{fw} < 8$ N · m/A;
- Flywheel charging volt/current limits: $V_{fwC} < 3{,}000$ V, $I_{fw\_C} < 200$ A;
- Flywheel discharge limits (DOD, depth of discharge): DOD = 85%; and
- Flywheel peak power (in simulations): $P = 54$ kW.

Flywheel Energy Storage—Regenerative Braking

Some simplifying assumptions are made in the following derivation of the regenerative-braking approach presented subsequently. These assumptions are used only to facilitate development of the feedback-based algorithm. The model used for the numerical examples does not incorporate these assumptions, thus providing a more realistic simulation. The term i_{brake} can be neglected because it will be very small under normal flywheel charging/discharging because of a large R_{brake} and properly sized flywheels. The flywheel drag term in Eq. (10) can also be neglected because the flywheel operates in a vacuum and is supported by magnetic bearings. The traction motor current and flywheel torque are given by

$$i_{tm} = 5 i_{fw} \tag{16}$$

$$T_{fw} = K_{fw} i_{fw} \tag{17}$$

The slug car's traction motor power and flywheel power are

$$P_{tm} = 6 T_{tm} \omega_{tm} = -6 K_{tm} 5 i_{fw} \omega_{tm} = -10 V_{tm} i_{fw} \tag{18}$$

$$P_{fw} = 10T_{fw}\omega_{fw} = 10K_{fw}i_{fw}\omega_{fw} = 10V_{fw}i_{fw} \tag{19}$$

The slug car's traction motor voltage and flywheel voltage are related by Kirchoff's voltage law as

$$V_{tm} - V_{fw} = 5i_{fw}(R_{tm} + R_{\text{cable}}) + i_{fw}R_{fw} + (5L_{tm} + L_{fw})\frac{di_{fw}}{dt} \tag{20}$$

The maximum current delivered to the flywheels by the traction motor generators is typically less than 1,000 A and will diminish within a period of 2–10 min during braking. The system is of a dc type, and it can be reasonably assumed that the flywheel charging current varies in a smooth and slow manner, at a rate similar with the train's speed variation. So it is assumed that the inductive voltage drop $[L(di/dt)]$ is negligible. This drop is included in the simulations but is omitted in this paper to facilitate development of the control algorithm. Eq. (20) then becomes

$$V_{tm} - V_{fw} = V_{tm} - K_{fw}\omega_{fw} = 5i_{fw}(R_{tm} + R_{\text{CABLE}}) + i_{fw}R_{fw} \tag{21}$$

The back emf of the flywheel increases as its speed is increased during charging. This reduces the net voltage that is available to drive current through the flywheel motor. This constraint is partially mitigated by varying the torque/current, or back emf/speed gain of the traction motor K_{tm} or of the flywheel K_{fw}. This is referred to as flux weakening (El-Refaie et al. 2004).

Two approaches for varying these gains are to change the stator field strength in electromagnet machines or to vary the flux path parameters, such as air gaps, through mechanical means for permanent magnet (PM) machines. Palazzolo et al. ["Shaftless flywheel," Provisional U.S. Patent Serial No. 61/382,769 (2010)] have developed an approach to vary K_{fw} between zero and its maximum design value for PM machines. This approach mechanically varies the depth of insertion of the stator coils into the rotor's PM field.

Maximum Regenerative-Braking Energy Recovery Method

An approach was developed to maximize the regenerative-braking energy harvested by the flywheels, by varying the voltage across each flywheel in a special manner. Eq. (15) shows that the flywheel voltage can be set to any desired value at a given flywheel speed, ω_{fw}, by changing K_{fw} using flux weakening. Suppose that it is desired to vary the flywheel voltage according to

$$V_{fw} = K_{fw} \times \omega_{fw} = k_{\text{FB}} \times V_{tm} \tag{22}$$

As explained in the Appendix I, the term k_{FB} is defined to maximize the total energy harvested by the flywheel during braking and varies continuously with V_{tm}. For the traction motor to power the flywheel, the following must be met: $0 < k_{\text{FB}} < 1$. The total energy recovery by the flywheels during regenerative braking is given by Eq. (49) as

$$E_{fw} = \int_0^{t_f} \{P_{fw}\}dt = \int_0^{t_f} 10V_{fw}i_{fw}dt = \text{const}\,2. - \int_0^{t_f} \{Mi_{fw} + Ni_{fw}^2 + H + QV_{fw} + RV_{fw}^2\}dt \tag{23}$$

E_{fw} is maximized when the integral in Eq. (23) is minimized. In Appendix I, Eq. (55) shows

$$\int_0^{t_f} \{Mi_{fw} + Ni_{fw}^2 + H + QV_{fw} + RV_{fw}^2\}dt = \int_{V_f}^{V_o} \frac{\hat{M}(1-k_{\text{FB}})V_{tm} + \hat{N}(1-k_{\text{FB}})^2V_{tm}^2 + H + Qk_{FB}V_{tm} + Rk_{FB}^2V_{tm}^2}{U(1-k_{FB})V_{tm} + WV_{tm} + XV_{tm}^2 + Y}dV_{tm} \tag{24}$$

The term in Eq. (24) will be minimized if its integrand is minimized, so that the following function is made stationary with respect to k_{FB}

$$f(V_{tm}, k_{\text{FB}}) = \frac{\hat{M}(1-k_{\text{FB}})V_{tm} + \hat{N}(1-k_{\text{FB}})^2V_{tm}^2 + H + Qk_{\text{FB}}V_{tm} + Rk_{\text{FB}}^2V_{tm}^2}{U(1-k_{\text{FB}})V_{tm} + WV_{tm} + XV_{tm}^2 + Y} \tag{25}$$

Appendix I [Eq. (66)] shows that the stationary condition is uniquely satisfied within the physical range of k_{FB} if

$$k_{\text{FB}} = \frac{-C_B + \sqrt{C_B^2 - 4C_AC_C}}{2C_A} \tag{26}$$

If the k_{FB} value falls in the range $0 < k_{\text{FB}} < 1$, then the second derivative of f is automatically positive when evaluated at the k_{FB} value in Eq. (26), and therefore, this k_{FB} yields a minimum value of f and a maximum value of E_{fw}. If the k_{FB} value does not belong in this range, then the function f varies monotonically within [0, 1] and is minimum at one of the limits $k_{\text{FB}} = 0$ or $k_{\text{FB}} = 1$, which must be determined by substitution.

The k_{FB} value as obtained previously yields the maximum harvested energy obtained from braking the train by this method and is utilized to obtain the required flywheel voltage, per Eq. (22): $V_{fw} = k_{\text{FB}} \times V_{tm}$.

Balanced Braking Regenerative Energy Recovery and Braking Effort Method

An effect of the previous approach is to reduce currents to reduce losses in the cabling. Lowering the currents also lowers the traction motor torques and consequently the braking forces. This leads to longer stopping distances, which may be impractical. The method shown subsequently is similar in principle to the linear quadratic regulator feedback controller in control theory, which seeks to reduce multiple objectives by minimizing a single cost function. The individual objectives cannot be minimized because of trade-offs between the competing objectives; however, an integrated

weighted sum of the objectives may be minimized. This expression becomes the sole objective to minimize.

The train's velocity is given by

$$v_{\text{train}} = \frac{R_{\text{wheel}}}{r_{\text{gear}}}\omega_{tm} = \frac{R_{\text{wheel}}}{3r_{\text{gear}}K_{tm}}V_{tm} \tag{27}$$

where r_{gear} is the gear ratio, and typically $r_{\text{gear}} \gg 1$.

The value of the total kinetic-energy power loss for the train, $P_{\text{kin loss}}$, is given by $(P_{\text{Davis}} - P_{tm})$, and the flywheel's harvested power is P_{fw}. Define the power-harvesting ratio as $P_{fw}/P_{\text{kin loss}} = P_{fw}/(P_{\text{Davis}} - P_{tm})$, which by utilizing Eqs. (6), (18), (19), and (27) becomes

$$\frac{P_{fw}}{P_{\text{kin loss}}} = \frac{10V_{fw}i_{fw}}{P_{\text{Davis}} - P_{tm}} = \frac{10[V_{tm} - (5R_{tm} + 5R_{\text{cable}} + R_{fw})i_{fw}]i_{fw}}{F_{\text{Davis}}v_{\text{train}} + 10V_{tm}i_{fw}}$$
$$= \frac{10[V_{\text{tm}} - (5R_{tm} + 5R_{\text{cable}} + R_{fw})i_{fw}]i_{fw}}{A\frac{R_{\text{wheel}}}{3r_{\text{gear}}K_{tm}}V_{tm} + B\left(\frac{R_{\text{wheel}}}{3r_{\text{gear}}K_{tm}}\right)^2V_{tm}^2 + C\left(\frac{R_{\text{wheel}}}{3r_{\text{gear}}K_{tm}}\right)^3V_{tm}^3 + 10V_{tm}i_{fw}} \tag{28}$$

The braking force supplied by the traction motors may be expressed utilizing Eq. (4) and Eq. (16) as

$$F_{\text{brake}} = -F_{\text{Slug Car}} = \frac{30K_{tm}i_{fw}r_{\text{gear}}}{R_{\text{wheel}}} = r_1 i_{fw} \tag{29}$$

where

$$r_1 = \frac{30K_{tm}r_{\text{gear}}}{R_{\text{wheel}}} \tag{30}$$

One objective is to increase the energy recovery efficiency expressed by Eq. (28). The second objective is to stop the train in an acceptable distance by increasing the braking force or from Newton's law by increasing the train's deceleration $F_{\text{brake}}/m_{\text{train}}$ (deceleration caused by slug car traction motor force). A single aggregate objective function, T, is defined as

$$T = \left(\frac{m_{\text{train}}}{F_{\text{brake}}}\right)^2 + b^2\left(\frac{P_{\text{kin loss}}}{P_{fw}}\right)^2 \tag{31}$$

This consists of the weighted sum of the inverses of these two objectives, with the energy recovery component including the weighting factor b, where $b > 0$. Only the function T is minimized; that is, the braking force and energy recovery are not independently maximized. This is a subjective approach because a decision maker must select b. The "Proof of Monotonicity of Solution" section in Appendix II demonstrates that the energy recovery efficiency is a monotonically increasing function of b and the braking effort is a monotonically decreasing function of b. This facilitates the task of the decision maker. Objective approaches as described by Deb (2001) and Deb et al. (2002) may also be employed, which utilize Pareto-compliant ranking methods, favoring nondominated solutions. The aggregate objective function (T) approach is a commonly used method, and the results presented in the numerical example section support the proposed approach, within the limits of the assumptions that the flywheel current is far greater than the current flowing through the braking resistor bank, and that the inductive voltage drop in Fig. 5 is negligible.

The flywheel charging current i_{fw} can be controlled by changing the K_{fw} as discussed previously. So the i_{fw} value was selected to be the optimization variable of the algorithm. Minimization of the function T [Eq. (31)] is discussed in detail in the "Maximum Regenerative-Braking Energy Recovery Method Solution" section in Appendix II.

The function Eq. (31) is shown to equal [Eq. (75)]

$$T(i_{fw}) = \frac{1}{i_{fw}^2}\left(\left(H + \frac{J^2}{L^2}\right) - 2\frac{J}{L}\left(I + \frac{JK}{L}\right)\frac{1}{K - Li_{fw}} + \left(I + \frac{JK}{L}\right)^2\left(\frac{1}{K - Li_{fw}}\right)^2\right) \tag{32}$$

The function T tends to $+\infty$ as i_{fw} tends to 0 and K/L, which, according to Eq. (21), corresponds to $V_{fw} = V_{tm}$ and $V_{fw} = 0$. So according to Rolle's theorem, there exists at least one local minimum for $T(i_{fw})$ within the range $i_{fw} \in (0, K/L)$.

The first derivative of $T(i_{fw})$ gives [Eq. (78)]

$$(HL^3 + J^2L)i_{fw}^3 + (3IJL - 3HKL^2)i_{fw}^2 + (2I^2L - IJK + 3HK^2L)i_{fw} - I^2K - HK^3 = 0 \tag{33}$$

Its discriminant is [Eq. (83)]

$$\Delta = 18C_aC_bC_cC_d - 4C_b^3C_d + C_b^2C_c^2 - 4C_aC_c^3 - 27C_a^2C_d^2 \tag{34}$$

If $\Delta \le 0$, Eq. (33) will only have one real root [Eq. (84)]. Appendix II proves that this root is the actual solution and its value is given by

$$i_{fw} = -\frac{C_b}{3C_a} - \frac{1}{3C_a}\sqrt[3]{\frac{1}{2}[2C_b^3 - 9C_aC_bC_c + 27C_a^2C_d + \sqrt{(2C_b^3 - 9C_aC_bC_c + 27C_a^2C_d)^2 - 4(C_b^2 - 3C_aC_c)^3}]}$$
$$- \frac{1}{3C_a}\sqrt[3]{\frac{1}{2}[2C_b^3 - 9C_aC_bC_c + 27C_a^2C_d - \sqrt{(2C_b^3 - 9C_aC_bC_c + 27C_a^2C_d)^2 - 4(C_b^2 - 3C_aC_c)^3}]} \tag{35}$$

When $\Delta > 0$, the other two real roots are given in Eqs. (85) and (86). All three roots will be evaluated with $T(i_{fw})$; the one that falls into $i_{fw} \in (0, K/L)$ and produces the smallest $T(i_{fw})$ will be selected as the solution

$$i_{fw\_2} = -\frac{C_b}{3C_a} + \frac{1 + i\sqrt{3}}{6C_a}\sqrt[3]{\frac{1}{2}[2C_b^3 - 9C_aC_bC_c + 27C_a^2C_d + \sqrt{(2C_b^3 - 9C_aC_bC_c + 27C_a^2C_d)^2 - 4(C_b^2 - 3C_aC_c)^3}]}$$
$$+ \frac{(1 - i\sqrt{3})(C_b^2 - 3C_aC_c)}{6C_a\sqrt[3]{\frac{1}{2}[2C_b^3 - 9C_aC_bC_c + 27C_a^2C_d + \sqrt{(2C_b^3 - 9C_aC_bC_c + 27C_a^2C_d)^2 - 4(C_b^2 - 3C_aC_c)^3}]}} \tag{36}$$

$$i_{fw\_3} = -\frac{C_b}{3C_a} + \frac{1 - i\sqrt{3}}{6C_a}\sqrt[3]{\frac{1}{2}[2C_b^3 - 9C_aC_bC_c + 27C_a^2C_d + \sqrt{(2C_b^3 - 9C_aC_bC_c + 27C_a^2C_d)^2 - 4(C_b^2 - 3C_aC_c)^3}]} + \frac{(1 + i\sqrt{3})(C_b^2 - 3C_aC_c)}{6C_a\sqrt[3]{\frac{1}{2}[2C_b^3 - 9C_aC_bC_c + 27C_a^2C_d + \sqrt{(2C_b^3 - 9C_aC_bC_c + 27C_a^2C_d)^2 - 4(C_b^2 - 3C_aC_c)^3}]}} \quad (37)$$

After the correct solution is found, the K_{fw} will vary according to Eq. (76)

$$K_{fw} = \frac{1}{\omega_{fw}}[V_{tm} - (5R_{tm} + 5R_{\text{cable}} + R_{fw})i_{fw}] \quad (38)$$

The constant b may be adjusted to balance the competing goals of increasing the amount of energy recovered during braking and stored in the flywheels, and stopping the train within an acceptable distance. This decision would ultimately involve a compromise between train scheduling and fuel-and NOx-reduction concerns.

Theoretically, both the amount of energy that will be harvested and the braking distance increase as b increases, unless b becomes exceedingly high causing i_{fw} to diminish and i_{brake} to become considerable, making the assumption that yielded Eq. (16) invalid.

Numerical Examples

Numerical simulations are provided in this section to illustrate the train-based, energy-storage/delivery flywheel system with regenerative-braking capability. Three different train operations are considered: (1) flywheel energy harvesting during regenerative braking, (2) flywheel line-haul service for energy transfer and NOx and fuel reduction, and (3) flywheel switcher service for energy transfer and NOx and fuel reduction. The same system of 10 flywheels and six traction motors is utilized for all simulations. It is notable that the simulations employed the modeling Eqs. (1)–(15) and did not employ the simplifying assumptions that were made to derive the energy-harvesting regenerative-braking approaches. This poses an additional challenge to the energy recovery approaches, which more closely reflects actual train operation. The successful outcome shown in the simulations confirms the effectiveness of the approaches.

The train and flywheel simulation parameters are shown in Table 1.

Train Regenerative-Braking Energy Harvesting

This section provides examples that confirm the effectiveness of the methods presented for increasing the amount of the train's kinetic energy transferred to rotational kinetic energy of the flywheels during braking. The first example utilizes fixed values of both K_{fw} and K_{tm}, and the second and third examples vary K_{fw} continuously during braking, using the maximum energy recovery and balanced energy recovery algorithms previously discussed. The latter two approaches yield significantly larger levels of recovered train energy that is transferred into the flywheels, even when compared with the best result of the constant K_{fw} approach.

Constant K_{fw} Approach

The slug car carries five pairs of counterrotating flywheels in this simulation of regenerative braking, which includes the train drag resistance (modified Davis) force, Eq. (6). The slug car traction motor gain (K_{tm}) has the constant value 3.5 N · m/A, and the flywheel motor gain was also kept constant to provide a benchmark to compare with the optimization methods. The total mass of the train with the flywheel slug car is 2.79×10^{-6} kg. The initial train velocity is 96 km/h, and kinetic energy is 276 kW · h. The individual flywheel stored energy is 20 kW · h (200 kW · h for all 10 flywheels) before the braking event occurs. Fig. 6 shows the recovered braking energy accumulated in the flywheel bank versus K_{fw} value.

The maximum energy recovered by the bank of 10 flywheels is approximately 98.0 kW · h at $K_{fw} = 1.2$ N · m/A. Fig. 7 shows the kinetic and dissipated energy variations during the braking process for $K_{fw} = 1.2$ N · m/A. As is shown, of the total initial kinetic energy of 276 kW · h, nearly 35.6% was recovered by the flywheels, 44.9% was wasted as electrical resistance (ohm) loss, 16.3% was dissipated because of the Davis force, and 3.3% was lost because of the final air braking after the speed reaches 17.6 km/h.

Fig. 8 shows that the final flywheel speed increases from 6,910 revolutions per minute (rpm) to 8,435 rpm during braking. The flywheel and slug car traction motor voltages and currents are plotted in Fig. 9. The traction motor voltages are always greater than those of flywheels during the flywheel charging phase, which indicates that the traction motors drive the flywheels by overcoming the flywheel emf voltage. The flywheel system stops charging and is removed from the circuit, and the resistor bank is inserted, when the flywheel emf voltage exceeds the traction motor voltage. This is indicated in the figure by setting the flywheel voltage to zero to indicate that the flywheel is removed from the circuit. Fig. 9 shows that nearly all of the traction motor current flows through the five flywheels, which supports the assumption made in deriving

Table 1. Simulation Parameters

Notation	Parameter	Value
M_{train}	Train mass without slug car (kg)	2,700,000
M_{slug}	Slug car mass with 10 flywheels (kg)	90,000
I_{fw}^{p}	Flywheel mass moment of inertia on z-axis (kg/m^2)	275
R_{wheel}	Train wheel radius (m)	0.5
L_{fw}	Flywheel inductance (H)	0.000011[a]
L_{tm}	Traction motor inductance (H)	0.000033[a]
R_{fw}	Flywheel resistance (Ω)	0.06
R_{tm}	Resistance of three traction motors (Ω)	0.18
R_{brake}	Brake bank resistance (Ω)	2,000
R_{cable}	Resistance of line connection (Ω)	0.3
K_{tm}	Slug car traction motor torque constant (N · m/A)	3.5
w	Weight per axle (kg)	22,500
n	Number of axles per car	4
W	Total car weight on rails (kg)	90,000
K_{air}	Air drag coefficient	0.07
r_{gear}	Traction motor gear ratio	62/15

[a]Varied up to 0.001 H on flywheel and 0.01 H on traction motors with negligible influence on recovered energy.

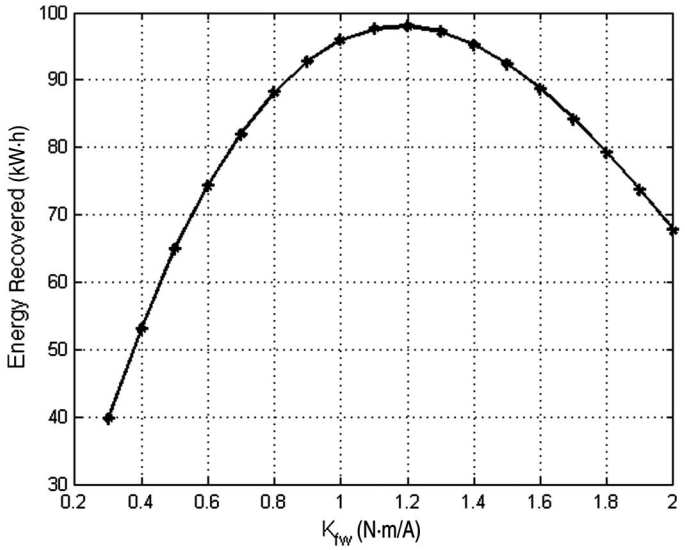

Fig. 6. Braking energy recovered by flywheel bank versus K_{fw} for the constant K_{fw} approach

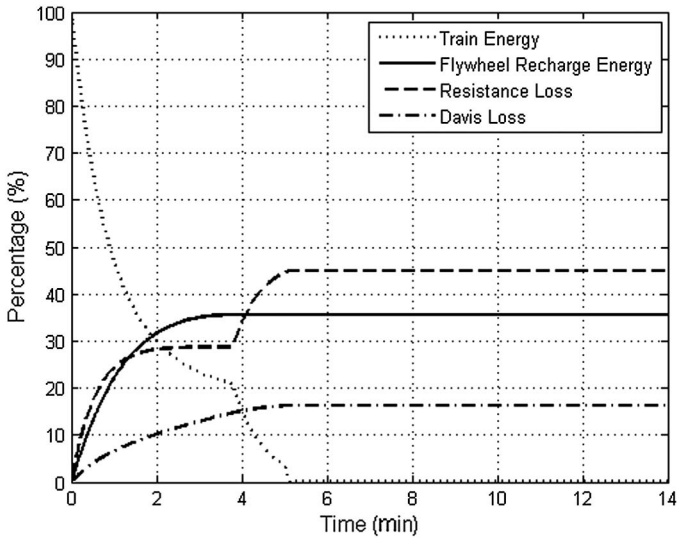

Fig. 7. Energy conversion for constant K_{fw}

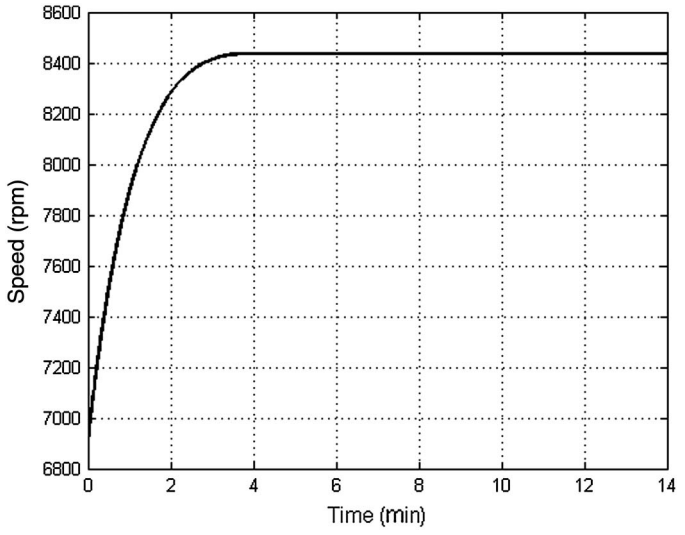

Fig. 8. Flywheel spin speeds for constant K_{fw}

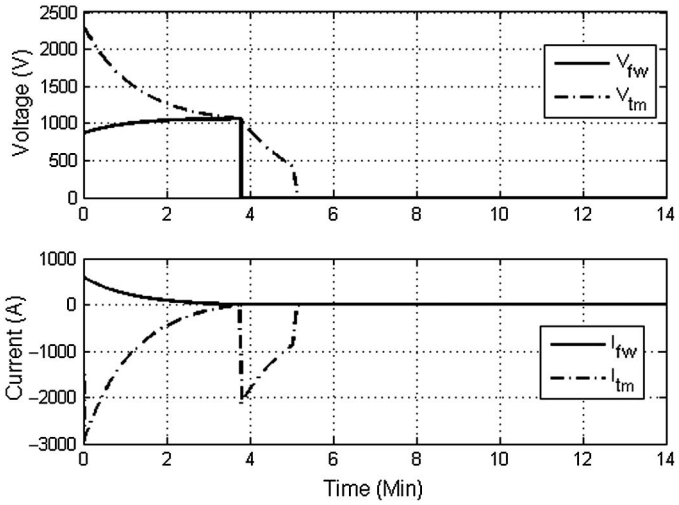

Fig. 9. Voltages and current for constant K_{fw}

Eq. (16). For instance, at $t = 0$, the traction motor current is 2,921.9 A, whereas the sum of all current flowing through the flywheels is 5×584.3 A $= 2,921.5$ A.

Maximum Energy Recovery Approach

The maximum energy recovery algorithm was used, and the simulation results were compared with the other two methods. The slug car traction motor gain (K_{tm}) stays constant at 3.5 N · m/A. Fig. 10 shows the kinetic and dissipated energy variations during the braking process. As is shown, of the total initial kinetic energy of 276 kW · h, approximately 55.0% was recovered by the flywheels, 12.0% was wasted as electrical resistance (ohmic) loss, 29.7% was dissipated because of the Davis force, and 3.3% was lost because of the final air braking after the speed reaches 17.6 km/h. An additional 19.4% of the total energy was harvested by the flywheels compared with the best constant K_{fw} method. This represents a 54.5% improvement in recovered energy over the best fixed K_{fw} case. In an absolute sense, the total energy recovered is 151.7 kW · h. The train velocity, distance, flywheel power,

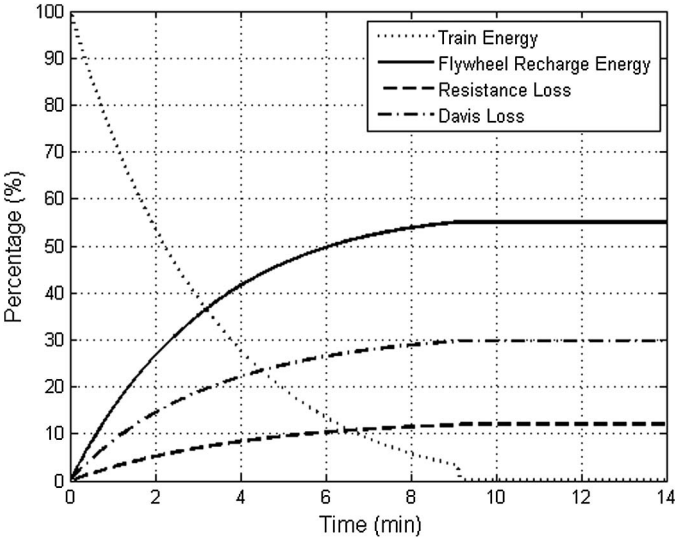

Fig. 10. Train energy conversion for maximum energy recovery approach

K_{fw} value, and recovered energy for all three approaches are compared with the other two cases in the following section.

Balanced Energy Recovery and Braking Effort Approach

The traction motor gain is set at $K_{tm} = 3.5$ N · m/A as in the other two approaches. Braking distance and energy recovery are plotted versus the weight factor b in Fig. 11. The maximum energy for all values of b is 152.8 kW · h, which is very close to that achieved with the maximum energy recovery approach (151.7 kW · h). Fig. 11 shows that the energy recovered can actually decrease with an increase of b value if b reaches a very high value. The flywheel charging currents reduce, and more current flows through R_{brake}, for these cases, which violates the assumption made to derive Eq. (16). Increasing R_{brake} causes the energy versus b curve to drop at a much higher b value with much slower slope. It is shown that, within a reasonable range, a change of b value successfully controls the energy recovery for the three approaches. The results comparing train velocity and distance, and flywheel power and K_{fw} value are shown in the Fig. 12 braking distance performance.

A b value of 36 was selected as shown in Fig. 13. The energy recovery values are compared in Fig. 14. As is shown, the balanced method with $b = 36$ can recover 151.9 kW · h of energy with a braking distance of 5.9 km. The energy recovered is very close to the 151.7 kW · h of energy recovered by the maximum energy method, which requires a braking distance of 7.5 km. This result is reasonable because the maximum energy method does not consider the braking effects and provides a solution similar to the balanced method for a high value of b. The best constant K_{fw} method recovers 98.0 kW · h with a braking distance of 4.3 km. As is shown in Fig. 11, the energy recovered for the best constant K_{fw} method is far worse than the balanced method with similar distance. A balance method with $b = 1$ will recover 136.6 kW · h of energy with a braking distance of 4.5 km.

Fig. 15 shows the voltages and currents for the flywheels and slug car traction motors. The initial currents are 949.4 A in the traction motors and 189.7 A in flywheels. The current values before air braking are 333.6 A in the traction motors and 63.0 A in the flywheels. This agrees well with the assumptions used to obtain Eq. (16) because $5 \times 66.7 = 333.5 \approx 333.6$ A (i.e., very little current flows through R_{brake}).

The distribution of the train's initial kinetic energy is shown in Fig. 16, showing that 55.1% of the train's initial kinetic energy

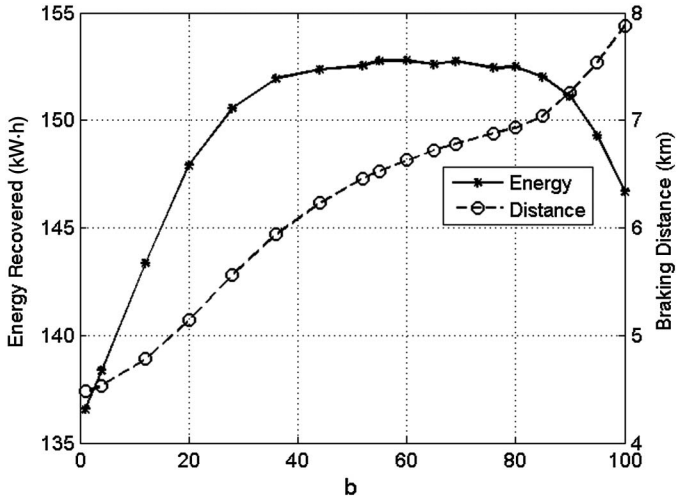

Fig. 11. Braking-energy recovery and distance for various values of b

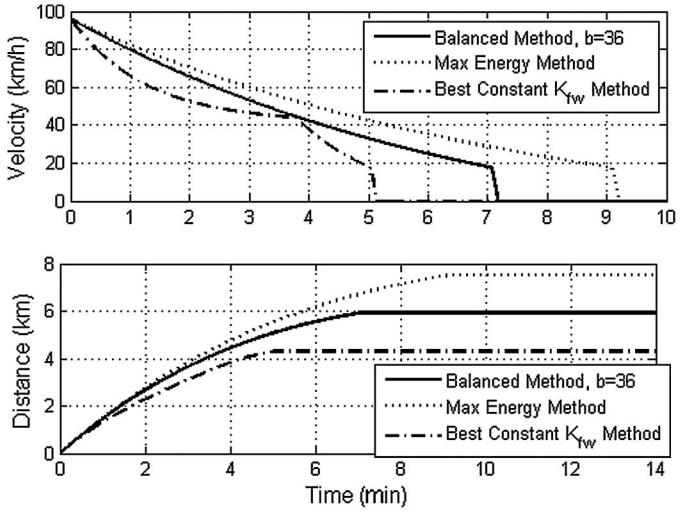

Fig. 12. Travel velocity and distance comparison for the three approaches

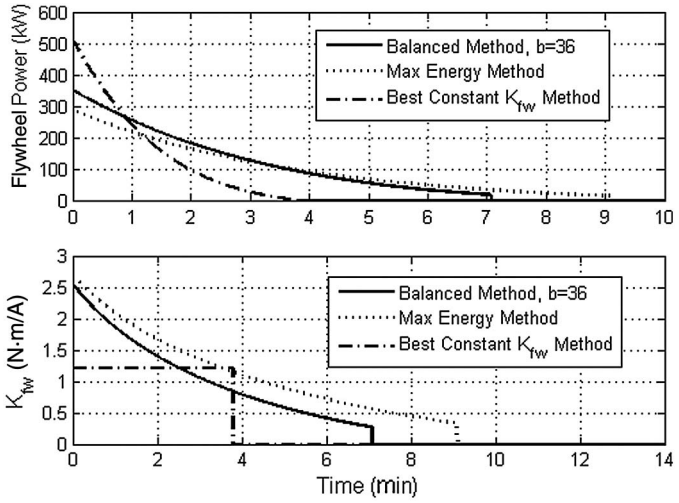

Fig. 13. Flywheel power and K_{fw} comparison for the three approaches

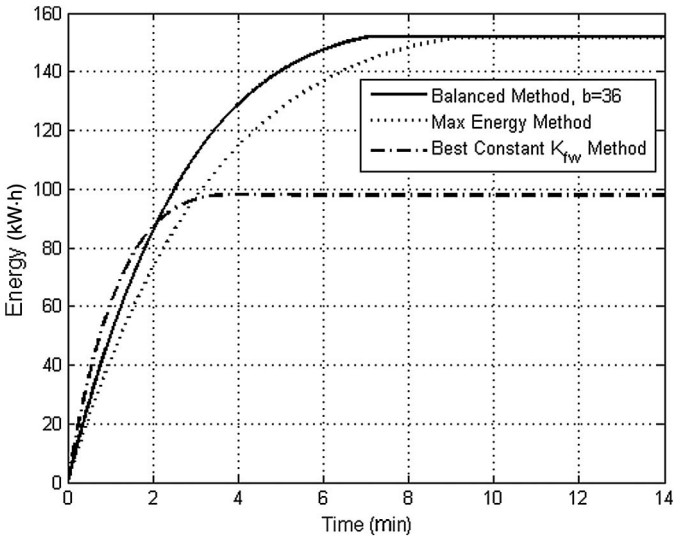

Fig. 14. Flywheel energy recovery comparison for the three approaches

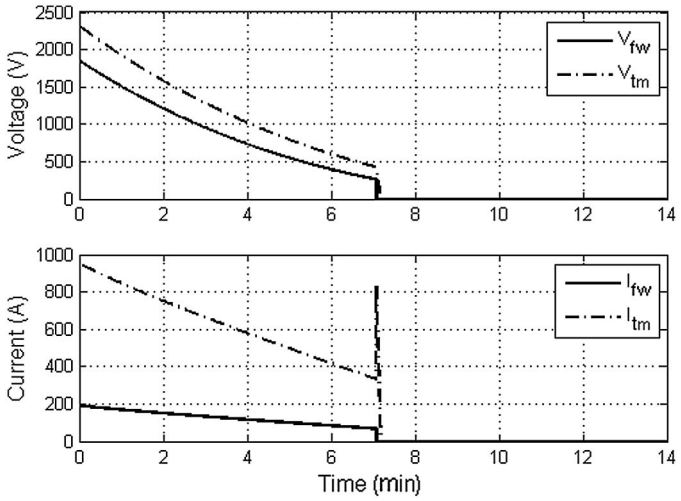

Fig. 15. Voltages and currents for balanced approach; $b = 36$

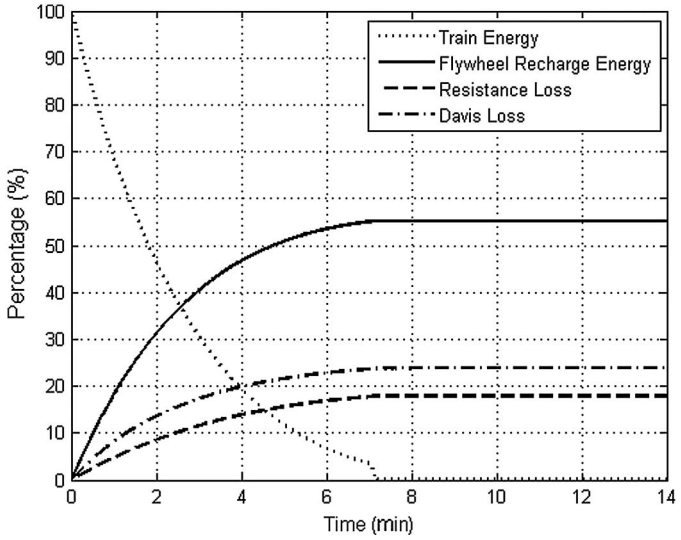

Fig. 16. Braking-energy conversion for balanced approach; $b = 36$

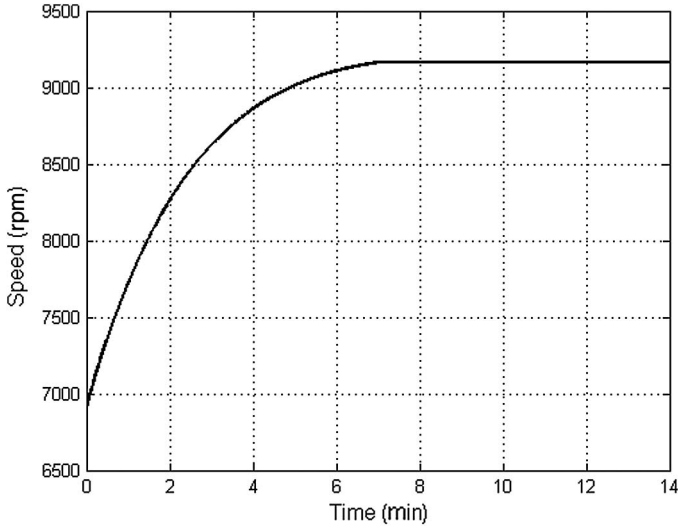

Fig. 17. Flywheel spin speed for balanced approach; $b = 36$

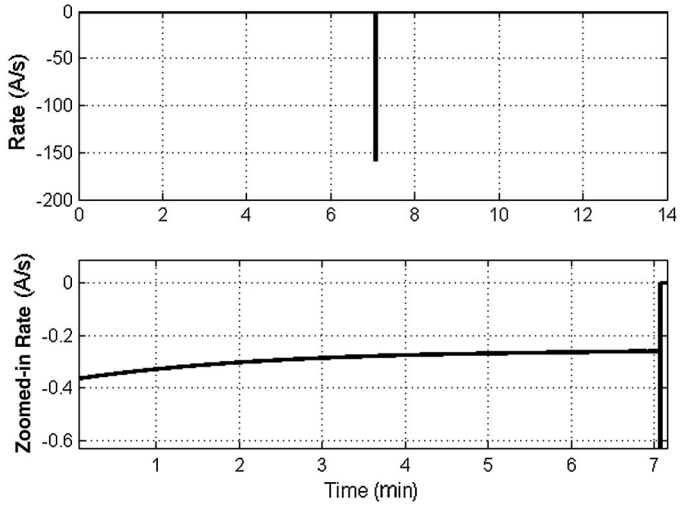

Fig. 18. Flywheel current change rate for balanced approach; $b = 36$

before braking is converted to flywheel spin kinetic energy, 23.7% is consumed by the Davis drag force, 17.9% is consumed by electrical resistance loss, and 3.3% is lost during air braking. Fig. 17 shows the flywheel spin speed, which increases from 6,910 rpm to 9,167 rpm during braking.

Fig. 18 shows the rate of change of flywheel current during the braking process. The current spike is an artifact of the initiation of air braking and is less than 200 A/s. The corresponding inductive voltage is less than 3 V, with an inductance limit value of $5L_{tm} + L_{fw} = 0.015$ H. During the whole operating time of the proposed algorithm, the peak current changing rate is less than 0.5 A/s, corresponding to an inductive voltage of less than 7.5 mV. This supports the assumption of negligible inductive voltage that was made in deriving Eq. (21).

Intuitively, the stored energy in the flywheel should increase with increasing K_{tm} because the traction motor voltage, which marks the capability of driving currents through the flywheels, is proportional to K_{tm}. Fig. 19 shows the maximum percentage of the original kinetic energy that can be recovered for different K_{fw}. The corresponding braking distance can also be found in Fig. 19. These charts indicate that the K_{tm} gain should be set at

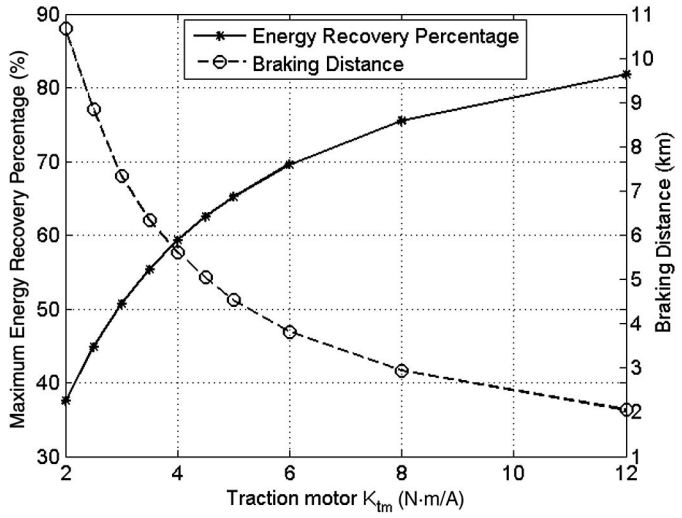

Fig. 19. Max energy recovery percentage and braking distance versus K_{tm} for balanced approach

its highest possible value for the best regenerative-braking results. Of course, the physical limitations for increasing K_{tm} need to be considered, such as the traction motor's field strength, eddy currents, current limits, and so forth.

As illustrated previously, the balanced energy recovery and braking effort algorithm and the maximum energy recovery algorithm both can achieve much higher energy recovery than the fixed K_{fw} approach. However, the balanced method can achieve a similar amount of energy recovery with much shorter braking distance because of the introduction of the acceleration term in the minimization target as Eq. (31). In addition to these, the balanced method will also give the train operator a real-time control over the importance of energy recovery and braking effectiveness under different situations. This is why the balanced energy recovery and braking effort algorithm is considered better and is utilized for the following line-haul and switcher simulations.

Hybrid Diesel/Flywheel Power Delivery for Line-Haul Power

The simulations performed in this section assume that the flywheels are initially charged from the local electric grids at the station and are also charged during operation by regenerative braking. In practice, the flywheels could be charged by the Diesel engines on the locomotives. However, this would require electrical connections between the slug car and Diesel locomotives and would produce much higher NOx emissions.

The flywheel system can deliver some or all of the train's power requirements at idle or at some of the train's power (notch) settings 1 through 8. The proposed slug car—Diesel locomotive approach separates the Diesel-powered propulsion from the flywheel-powered propulsion because they use different sets of traction motors. For instance, this would allow use of a dc flywheel—dc traction motor slug car and ac Diesel locomotives on the same train.

Sierra Research Inc. (2004) provides an average train power and NOx emissions schedule based on considering the myriad of routes and schedules occurring in the United States. This provides the Diesel engine—only operation data to compare with the hybrid power approach. Table 2 presents the EPA's average line-haul schedule, derived from page A-5 of the Sierra Research Inc. report, which is in turn obtained from EPA (1998) and Fritz (2000). All the data were converted from U.S. units into SI units. With reference to Table 2, all trains operate in one of eight power (notch) settings, in idle or in braking.

The paper presents estimates of the total fuel F_u (in liters) consumed for hybrid powering of the train by integrating curve fits of dF_u/dt and the total mass M_N (in kilograms) of NOx emitted by integrating curve fits of dM_N/dt, as obtained from Table 2. Both dF/dt and dM_N/dt are curve fitted in terms of the Diesel power in kW.

Table 3 is derived from the data in Table 2 and lists the amount of Diesel fuel consumed and NOx emitted for three special cases. The first case is a reference case in which the Diesel locomotive supplies power in all states of operation. The second and third cases show the amount of fuel and NOx for a reduced schedule, which excludes notches 7 and 8 (second case), or only notch 8 (third case). In a converse sense, the table provides the amount of fuel that is saved and the amount of NOx that is not emitted if the bank of flywheels supplies all of the power for the following:

- Case 2: power settings 1–6, plus idle and brake; and
- Case 3: power settings 1–7, plus idle and brake.

Clearly, Table 3 shows that if the precharged 10-flywheel cluster supplied all of the power for idle and notches 1–6 or 1–7, the NOx emissions and fuel consumption would be reduced by more than 30%. Supplying the lower power settings (1–6 or 1–7) and idle with the flywheel power is particularly advantageous because the Diesel's efficiency is reduced at these lower power settings. This is illustrated by Fig. 20, which shows a plot of the work (energy) performed by the Diesel engine per unit of fuel versus engine load factor, as taken from Table 2. Table 3 estimates that 269 kW · h and 346 kW · h of flywheel stored energy would need to be delivered during the EPA average 1-h line-haul operation. The simulations show that a large portion of this is recovered from regenerative braking so that the flywheel system can continue to supply sufficient energy to reduce NOx emissions and fuel consumption by the amounts shown in Table 3 for multiple 1-h EPA cycles.

As discussed previously, the drag force called the modified Davies formula [Eq. (6)] was utilized to model various forms of losses. Extensive simulations have been conducted for a 2.79×10^{-6} kg train, which includes a Diesel engine–driven locomotive and a flywheel slug car with its own set of traction motors plus 10 flywheels. Assuming that the efficiency of the Diesel locomotive system is 75%, the force F_{diesel} driving the Diesel can be retrieved as in Eq. (4) utilizing various power levels (minus the idle power) shown in Table 2 $P_{\text{diesel}} = 0.75(P_{\text{notch}\,N} - P_{\text{idle}})]$. The

Table 2. EPA's Average Line-Haul Schedule

Diesel power setting (DPS)	Notch fuel rate (L/h)[a] dF_u/dt	Power (kW)	Fuel energy density (kW · h/L)	Engine load factor[b]	Line-haul weight (%)[c]	Fuel in 1 h (L)[d]	Energy in 1 h (kW · h)[d]	Notch NOx rate (kg/h)[a] dM_N/dt	NOx in 1 h (kg)[d]
Brake	87.1	88.4	1.01	0.028	12.5	10.88	11.1	1.34	0.17
Idle	16.7	18.7	1.12	0.0061	38.0	6.34	7.1	0.31	0.12
1	40.5	145.5	3.59	0.0475	6.5	2.63	9.5	1.30	0.08
2	89.3	298.4	3.34	0.0975	6.5	5.80	19.4	3.0	0.20
3	199.1	708.7	3.55	0.231	5.2	10.35	36.9	7.3	0.38
4	272.9	1,044.4	3.83	0.341	4.4	12.01	46.0	14.0	0.62
5	392.2	1,529.3	3.90	0.50	3.8	14.90	58.1	25.6	0.97
6	501.6	2,066.4	4.12	0.675	3.9	19.56	80.6	33.6	1.31
7	611.7	2566	4.19	0.839	3.0	18.35	77.0	39.8	1.19
8	733.6	3,058.6	4.17	1.000	16.2	118.84	495.5	47.0	7.61
						219.66	841.2		12.65

Note: Adapted from Sierra Research Inc. (2004); converted to SI units.
[a]For the given Diesel power settings.
[b]Fraction of full engine power.
[c]Percent of time at given Diesel power setting.
[d]For the given DPS and line-haul weight.

Table 3. Diesel Engine Fuel Consumption and NOx Emissions

Power setting schedule	For all Diesel power settings	For settings 1–6, plus idle and brake	For settings 1–7, plus idle and brake
Fuel consumed per hour (L) (percentage of total)	219.66 (100)	82.48 (37.55)	100.83 (45.90)
NOx emitted per hour (kg) (percentage of total)	12.65 (100)	3.85 (30.43)	5.04 (39.84)
Diesel energy utilized per hour (kW · h) (percentage of total)	841.2 (100)	268.7 (31.94)	345.7 (41.10)

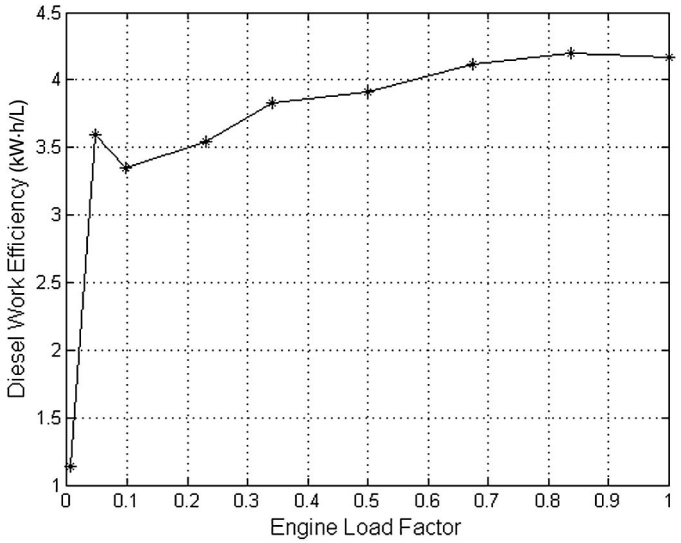

Fig. 20. Diesel work per fuel versus engine load factor

value of 75% efficiency is consistent with William (1982) who recommends 82% minus additional losses for journal and rolling resistance. The model is based on the electromechanical equations and braking recovery algorithms previously presented. An analogous inefficiency is included in the flywheel charge and discharge models through the resistive losses in the cables. The resistance loss varies depending on flywheel charge/discharge currents and is approximately 21% during the hybrid line-haul simulation shown subsequently.

It is assumed that each of the 10 flywheels have received an initial charge at the station of 54 kW · h of kinetic energy, at a rotational speed of 11,355 rpm, and with individual flywheel inertia of 275 kg/m^2. The two areas investigated are (1) the demonstration of NOx and fuel reductions compared with Diesel-only operation and (2) demonstration of energy harvesting based on regenerative braking. The following simulations are for two different train power-sharing scenarios indicated by Case 1 and Case 2. The fuel consumption and NOx emissions are compared between the two cases. The Diesel power time schedule for each notch setting is presented in Table 4.

Case 1—Diesel Engine Only

A 2.79 × 10 kg^{-6} train, without slug car, follows the EPA's average power schedule (line-haul weight and Diesel power setting) described in Tables 2 and 4, including the idle time, and is simulated for a 1-h trip. Figs. 21 and 22 show that after idling for approximately 23 min, the train travels for approximately 31.0 km and has a maximum velocity of approximately 100.7 km/h, followed by a braking period. The corresponding fuel consumption and NOx emissions are shown as 216.0 L and 12.4 kg, respectively. The slight discrepancy between these values and Table 3 is attributable to error in the curve-fitting functions for the data in Table 2, which are used for calculating emissions and fuel usage.

Case 2—Hybrid Flywheel/Diesel Power for Three Consecutive, 1-h EPA Cycles

This case considers a 10-flywheel energy-storage system, with each flywheel initially charged with 54 kW · h of energy and the flywheel system supplying all of the power for idle and power notch settings 1–6. The Diesel locomotive provides power for notch settings 7 and 8, which are the most efficient power settings for the Diesel engine. A 90,000-kg slug car carrying a 10-flywheel cluster was added to the train simulation model. The traction motor gain is fixed at 3.5 N · m/A, and the balanced energy recovery and braking effort method was used for this hybrid power example with $b = 36$. The maximum speed and travel distance in a single cycle are 99.5 km/h and 31.1 km, respectively, as shown in Fig. 23. The distance is a little longer than the pure Diesel power case because of the longer braking distance.

Fig. 24 shows the amount of fuel consumption and NOx emissions with the 10-flywheel cluster, resulting in final values of 427.9 L and 26.1 kg, respectively. By multiplying the single EPA cycle results for pure Diesel power by a factor of 3 in Fig. 22 (3 × 216.0 LL = 648.0 L, 3 × 12.4 kg = 37.2 kg), the reductions achieved with hybrid power are fuel, 34.0% (220.1 L), and NOx, 29.8% (11.1 kg). Given the EPA's (2005) CO_2 emission data for Diesel fuel (2.668 kg/L), 587.2 kg of CO_2 can also be reduced during the whole process. The flywheel spin speed was decreased to approximately 7,627 rpm from its initial 11,355 rpm, after three regenerative-braking boosts shown in Fig. 25. The lowest flywheel spin speed during the whole process is 4,446 rpm, which occurs just before the final regenerative-braking event. The voltages and currents in the electric-mechanical system are presented in Fig. 26. During the flywheel energy delivery period (train is propelled by the 10-flywheel cluster), the voltage of the flywheel system is always higher than that of the train traction motor. In contrast, the traction motor voltage is higher than flywheel system voltage during regenerative-braking service (train traction motors drive flywheels). The currents are negative for flywheel energy delivery, and

Table 4. Diesel Power Time Intervals at Given Notch Settings

	Notch number										
Time (s)	Idle	1	2	3	4	5	6	7	8	Brake	Final time
t_i	0	1,368	1,602	1,836	2,023	2,182	2,318	2,459	2,567	3,150	3,600
Δt	1,368	234	234	187	158	137	140	108	583	450	

Note: Case 1 = only Diesel engine power for idling and all power notch settings (1–8); no flywheels. Case 2 = power from 10 flywheels with initial total energy of 540 kW · h utilized for idle and power notch settings 1–6; Diesel engine power for power notch settings 7 and 8; hybrid power mode.

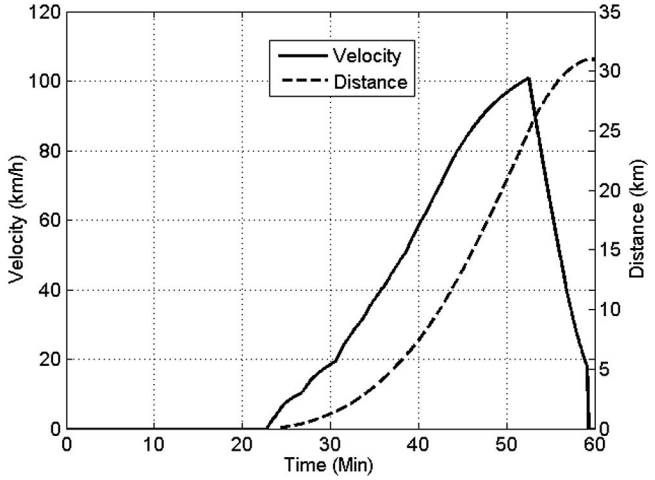

Fig. 21. Train travel velocity and total distance

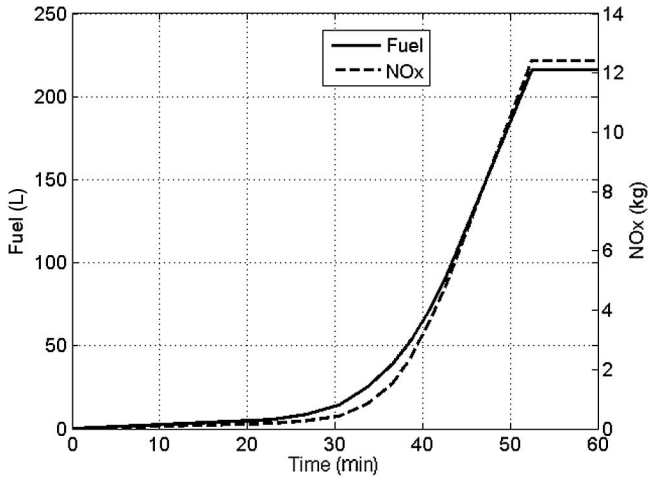

Fig. 22. Total fuel consumption (L) and total NOx emissions (kg)

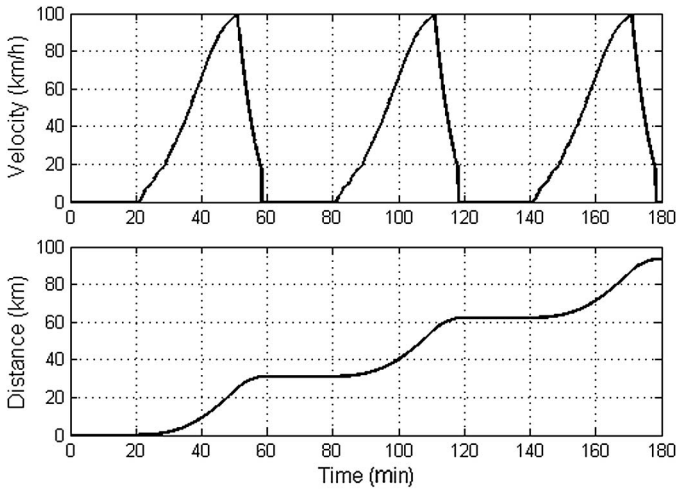

Fig. 23. Train travel velocity and distance

positive for flywheel energy charging as shown in Fig. 26. The power in an individual flywheel and individual traction motor is shown in Fig. 27. Without losses, the power of a traction motor should be approximately 1.667 times the power of a flywheel

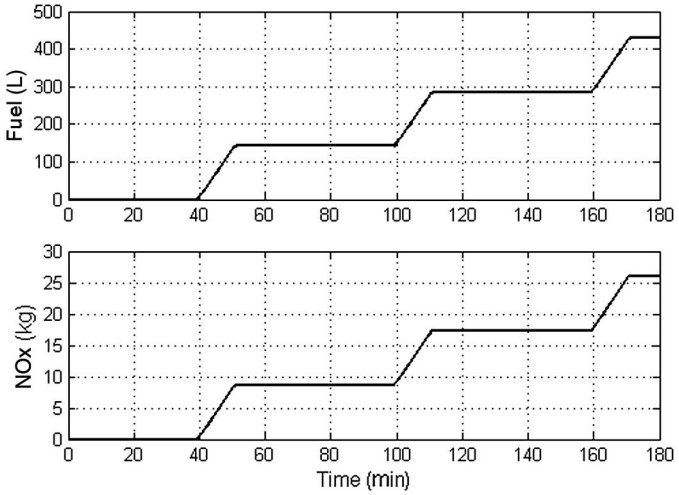

Fig. 24. Total fuel consumption and total NOx emissions

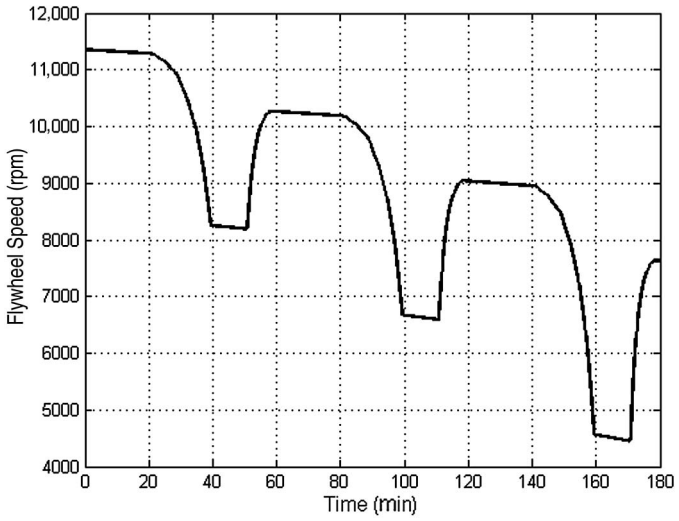

Fig. 25. Flywheel spin speeds

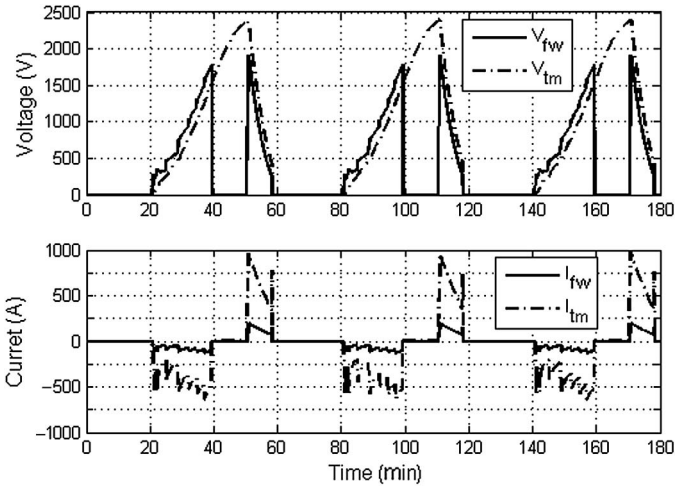

Fig. 26. Voltages and currents in individual flywheels and individual traction motors

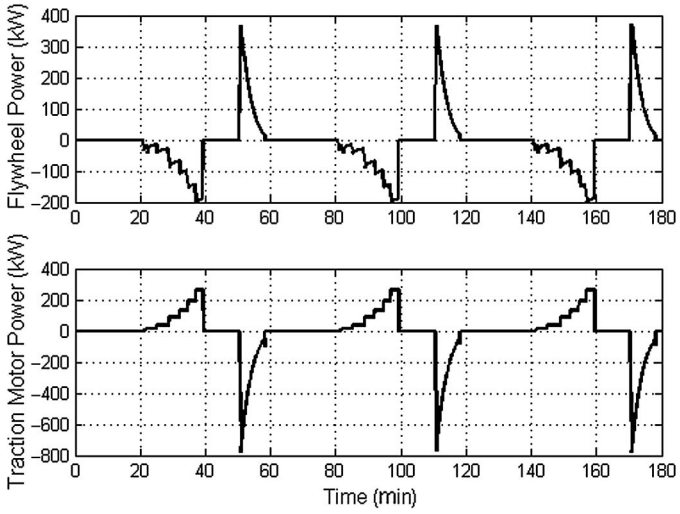

Fig. 27. Flywheel and traction motor power

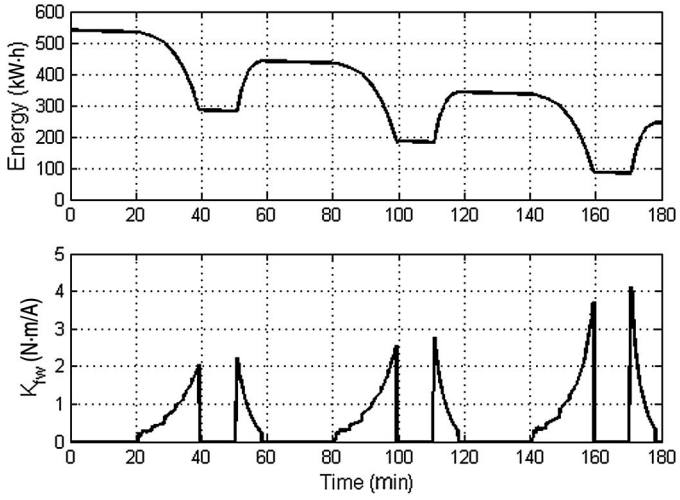

Fig. 28. Flywheel energy transfer and K_{fw}

because there are five flywheels and three traction motors in each group. However, because of resistance losses, the traction motor power is lower than that value when the flywheel delivers power to the traction motor, and higher than that value when the traction motor is charging the flywheel. The total energy transfer of the 10-flywheel cluster is shown in 28. The flywheel cluster was initially charged to 540 kW · h and expends approximately 259.2 kW · h to power notch settings 1–6 and idle, for the first EPA cycle. This energy does not contain the energy needed for the Diesel engine during braking, which is included in the data in Table 4, because the flywheel-powered slug system does not need to supply this power. Thus, the energy supplied by the flywheel is slightly less than the 268.7 kW · h of energy listed in Table 4 as the summation of notch 1 ~ 6, idle, and braking.

The regenerative braking recovers approximately 160.8 kW · h of energy to charge the flywheel, after each cycle. After three cycles of operation, the remaining energy of the flywheel cluster is 243.6 kW · h. The flywheel gain constant K_{fw} is time varying as depicted in Fig. 28. As is shown, the later cycles requires higher K_{fw} values because the flywheel spin speed has been reduced, but the flywheel power delivery requirement still remains the same.

All-Electric Flywheel System for Switcher Power

Sierra Research Inc. (2004) also provides average switcher service duty cycles as given in Table 5. The switcher operates only in the switchyard, so it is located where electric power is easily accessible. The simulation study shown subsequently considers all-electric (flywheel) power service for two 1-h cycles.

The simulation assumes that the 10 flywheels were charged initially to 540 kW · h at the switchyard. The flywheel cluster energy is enough for the system to run for 2 h continuously. Train distance and speed plots are shown in Fig. 29. The travel distance in 2 h is 25.4 km with a maximum speed of 61.5 km/h. The EPA schedule did not provide a braking time, so 14% (5 min) of the idle time was used for braking during the simulations. Because no Diesel power is used, the net reductions are 152.2 L of fuel, 406.1 kg of CO_2, and 7.0 kg of NOx emissions. The flywheel spin speed is plotted in Fig. 30, showing that the final speed is approximately 5,795 rpm after regenerative-braking operations. The voltages and currents are presented in Fig. 31, and the flywheel and traction motor power curves are shown in Fig. 32. The flywheel system energy and time-varying flywheel motor/generator gain constant (K_{fw}) are plotted in Fig. 33. The final flywheel energy after 2 h of operation is 140.9 kW · h.

Table 5. EPA's Average Switcher Schedule

Diesel power setting (DPS)	Notch fuel rate (L/h)[a] dF_u/dt	Power (kW)	Fuel energy density (kW · h/L)	Engine load factor[b]	Switcher weight (%)[c]	Fuel in 1 h (L)[d]	Energy in 1 h (kW · h)[c]	Notch NOx rate (kg/h)[a] dM_N/dt	NOx in 1 h (kg)[d]
Brake	87.1	88.4	1.01	0.028	0	0	0	1.34	0
Idle	16.7	18.7	1.12	0.0061	59.8	9.99	11.18	0.31	0.19
1	40.5	145.5	3.59	0.0475	12.4	5.02	18.04	1.30	0.16
2	89.3	298.4	3.34	0.0975	12.3	10.98	36.70	3.0	0.37
3	199.1	708.7	3.55	0.231	5.8	11.55	41.10	7.3	0.42
4	272.9	1,044.4	3.83	0.341	3.6	9.82	37.60	14.0	0.50
5	392.2	1,529.3	3.90	0.50	3.6	14.12	55.05	25.6	0.92
6	501.6	2,066.4	4.12	0.675	1.5	7.52	31.00	33.6	0.50
7	611.7	2566	4.19	0.839	0.2	1.22	5.13	39.8	0.08
8	733.6	3,058.6	4.17	1.000	0.8	5.87	24.47	47.0	0.38
						76.09	260.27		3.52

Note: Adapted from Sierra Research Inc. (2004).
[a]For the given Diesel power setting.
[b]Fraction of full engine power.
[c]Percent of time at given Diesel power setting.
[d]For the given DPS and line-haul weight.

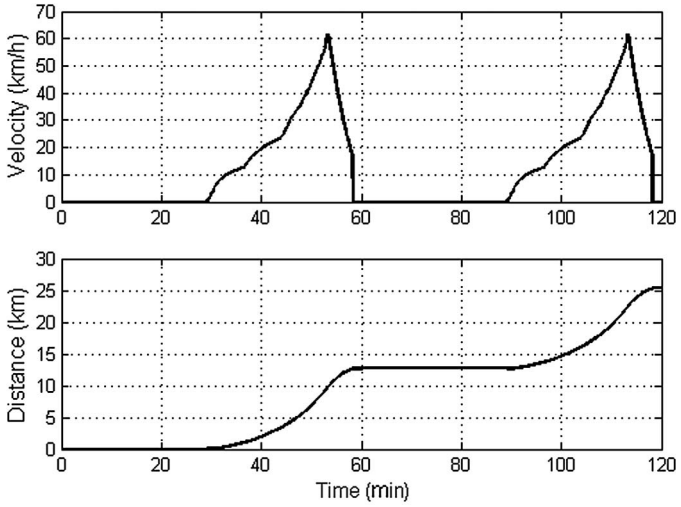

Fig. 29. Train velocity and distance

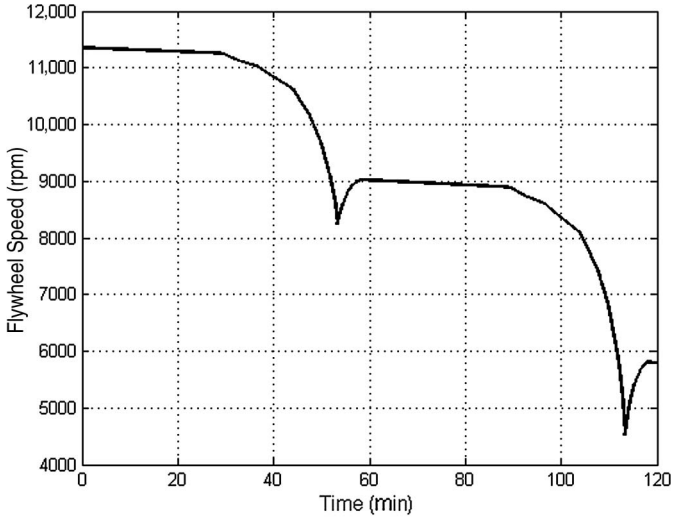

Fig. 30. Flywheel spin speeds

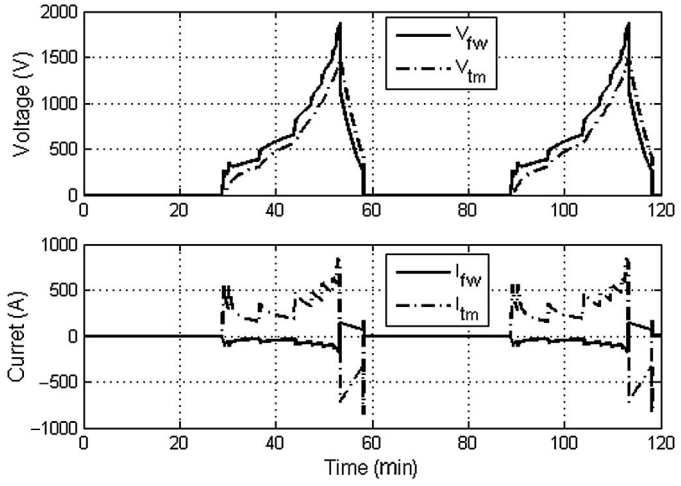

Fig. 31. Voltages and currents in electric circuit

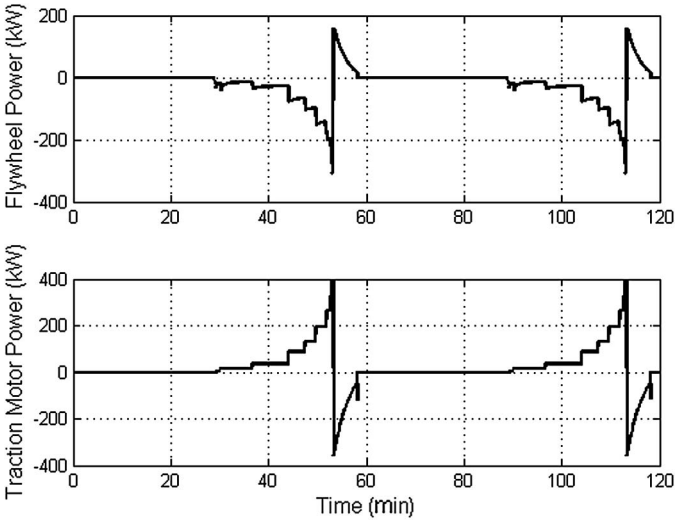

Fig. 32. Flywheel and traction motor power

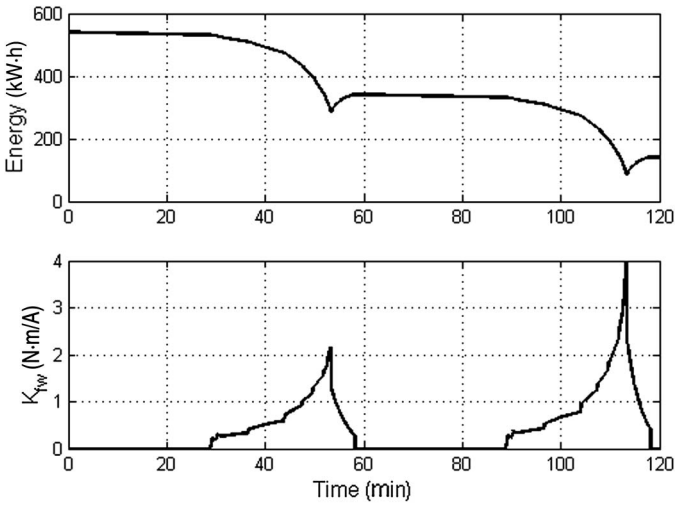

Fig. 33. Flywheel stored energy and K_{fw}

Discussion and Summary

The paper has introduced a novel concept of utilizing slug car–borne flywheels as portable power sources for train propulsion. The bank of flywheels will be charged from grid connection at rail yards and from regenerative braking. Power provided by the flywheels supplements power delivered by conventional Diesel locomotives to form a hybrid power source for operating the train. The benefits of this technology were evaluated through simulations, which showed potential fuel and NOx-emission reductions of approximately 30% relative to all Diesel power, line-haul operation of the train. This result is based on average train operation duty cycles published by the EPA. Simulation of a switcher showed the capability of the switcher to operate for 2 h of average EPA switcher service, powered solely on a flywheel bank that is initially charged to 540 kW · h. The hybrid flywheel–Diesel engine performance including train velocity and travel distance are almost identical to trains powered solely by a Diesel engine. Table 6 summarizes some of the numerical results presented in the previous sections.

Novel operation algorithms were developed to maximize harvesting of the total braking energy or to increase the harvested

Table 6. Summaries of Numerical Results in Previous Examples

Case	Train weight (10^6 kg)	Train power sharing		Max speed (km/h)	Travel distance per cycle (km)	NOx emission per cycle (kg)	Fuel consumption per cycle (L)
		Flywheel	Diesel				
Case 1	2.7	None	Idle, notch 1–8	100.7	31.0	12.4	216.0
Case 2	2.79	Idle, notch 1–6	Notch 7–8	99.5	31.1	8.7	142.6
Switcher case	2.79	Idle, notch 1–8	None	61.5	25.4	0	0

braking energy while also limiting the braking distance and time. Numerical examples were presented that confirmed the efficacy of the algorithms. A flux-weakening approach was shown to enable these algorithms through providing an ability to control flywheel voltage or current.

Future Work

An objective approach as described by Deb (2001) and Deb et al. (2002) will be employed, which utilizes Pareto-compliant ranking methods, favoring nondominated solutions, for the balanced regenerative-braking energy recovery and braking effort method. Implementation of the concepts presented and analyzed will require specific flywheel designs that are reliable, robust, and affordable. The authors are preparing a paper that describes a novel shaftless flywheel concept to meet these objectives. Developing an approach that will integrate the flywheels with the locomotive's Diesel generator set and traction motors will further reduce the cost for implementing the portable energy-storage flywheel concept. This work will include detailed power-conversion architectures to interface with ac and dc machinery. Hardware for implementing the flux-weakening approach described in the paper will be developed for both electromagnet and permanent-magnet flywheel motor generators. Finally, pending funding availability, a prototype of the technology described will be built and tested on a train.

Appendix I. Maximum Regenerative-Braking Energy Recovery Method

Inserting the modified Davis force Eq. (6) into the train equation of motion given by Eq. (1) and Eq. (3) yields

$$-m\frac{dV_{\text{train}}}{dt} = -m\frac{R_{\text{wheel}}}{r_{\text{gear}}}\frac{d\omega_{tm}}{dt} = -\frac{r_{\text{gear}}}{R_{\text{wheel}}}6T_{tm} + A + BV_{\text{train}} + CV_{\text{train}}^2 = \frac{r_{\text{gear}}}{R_{\text{wheel}}}K_{tm}30i_{fw} + A + B\frac{R_{\text{wheel}}\omega_{tm}}{r_{\text{gear}}} + C\frac{R_{\text{wheel}}^2}{r_{\text{gear}}^2}\omega_{tm}^2 \tag{39}$$

Because $\omega_{tm} = V_{tm}/3K_{tm}$ (three traction motors in series as in Fig. 5)

$$-\frac{dV_{tm}}{dt} = \left(\frac{r_{\text{gear}}}{R_{\text{wheel}}}\right)^2\frac{90K_{tm}^2}{m}i_{fw} + \frac{3K_{tm}r_{\text{gear}}}{mR_{\text{wheel}}}A + \frac{B}{m}V_{tm} + C\frac{R_{\text{wheel}}}{mr_{\text{rear}}}\frac{V_{tm}^2}{3K_{tm}} \tag{40}$$

Integrate Eq. (40) until the air brakes are engaged. The air brake speed (~5 m/s) occurs when the traction motor braking ceases and the train is brought to rest with air brakes

$$\int_0^{t_f}\left(-\frac{dV_{tm}}{dt}\right)dt = \int_0^{t_f}\left(\left(\frac{r_{\text{gear}}}{R_{\text{wheel}}}\right)^2\frac{90K_{tm}^2}{m}i_{fw} + \frac{3K_{tm}r_{\text{gear}}}{mR_{\text{wheel}}}A + \frac{B}{m}V_{tm} + C\frac{R_{\text{wheel}}}{mr_{\text{rear}}}\frac{V_{tm}^2}{3K_{tm}}\right)dt = V_{tmo} - V_{tmf} = \text{const.} \tag{41}$$

where V_{tmo} = initial traction motor voltage; and V_{tmf} = traction motor voltage when air braking is engaged. Because V_{tm} is proportional to the traction motor speed, it has fixed values for a given initial braking speed and an air braking speed. Substituting Eq. (21) yields

$$\int_0^{t_f}\left[\left(\frac{r_{\text{gear}}}{R_{\text{wheel}}}\right)^2\frac{90K_{tm}^2}{m}i_{fw} + \frac{B(V_{fw} + (5R_{tm} + 5R_{\text{cable}} + R_{fw})i_{fw})}{m} + C\frac{R_{\text{wheel}}}{mr_{\text{gear}}}\frac{(V_{fw} + (5R_{tm} + 5R_{\text{cable}} + R_{fw})i_{fw})^2}{3K_{tm}}\right]dt + \int_0^{t_f}\frac{3K_{tm}r_{\text{gear}}}{mR_{\text{wheel}}}Adt = \text{const.} \tag{42}$$

Define

$$M = \left(\frac{r_{\text{gear}}}{R_{\text{wheel}}}\right)^3\frac{1{,}350K_{tm}^3}{C(5R_{tm} + 5R_{\text{cable}} + R_{fw})} + \frac{15Br_{\text{gear}}K_{tm}}{CR_{\text{wheel}}} \tag{43}$$

$$N = 5(5R_{tm} + 5R_c + R_{fw}) \tag{44}$$

$$H = \frac{45}{C(5R_{tm} + 5R_{\text{cable}} + R_{fw})}\left(\frac{K_{tm}r_{\text{gear}}}{R_{\text{wheel}}}\right)^2 A \tag{45}$$

$$Q = \frac{15Br_{\text{gear}}K_{tm}}{C(5R_{tm} + 5R_c + R_{fw})R_{\text{wheel}}} \tag{46}$$

$$R = \frac{5}{(5R_{tm} + 5R_c + R_{fw})} \tag{47}$$

Eq. (42) becomes

$$\int_0^{t_f}(Mi_{fw} + Ni_{fw}^2 + H + QV_{fw} + RV_{fw}^2 + 10V_{fw}i_{fw})dt = \text{const.} \cdot \frac{15mr_{\text{gear}}K_{tm}}{C(5R_{tm} + 5R_{\text{cable}} + R_{fw})R_{\text{wheel}}} = \text{const2.} \tag{48}$$

The total energy recovered by the flywheel during the braking equals the integral of the total flywheel charging power given by Eq. (19)

$$E_{fw} = \int_0^{t_f}P_{fw}dt = \int_0^{t_f}10V_{fw}i_{fw}dt = \text{const2.} - \int_0^{t_f}(Mi_{fw} + Ni_{fw}^2 + H + QV_{fw} + RV_{fw}^2)dt \tag{49}$$

V_{tm} must be higher than V_{fw} during regenerative braking, so that $0 \le k_{\text{FB}} \le 1$. Eq. (39) may be written

$$\frac{dV_{tm}}{dt} = -\left(\frac{r_{\text{gear}}}{R_{\text{wheel}}}\right)^2 \frac{90K_{tm}^2}{m} i_{fw} - \frac{3K_{tm}r_{\text{gear}}}{mR_{\text{wheel}}}A - \frac{B}{m}V_{tm} - C\frac{R_{\text{wheel}}}{mr_{\text{gear}}}\frac{V_{tm}^2}{3K_{tm}}$$
$$= -\left(\frac{r_{\text{gear}}}{R_{\text{wheel}}}\right)^2 \frac{90K_{tm}^2}{m}\frac{1-k_{\text{FB}}}{(5R_{tm}+5R_{\text{cable}}+R_{fw})}V_{tm} - \frac{3K_{tm}r_{\text{gear}}}{mR_{\text{wheel}}}A - \frac{B}{m}V_{tm} - C\frac{R_{\text{wheel}}}{mr_{\text{gear}}}\frac{V_{tm}^2}{3K_{tm}} = -U(1-k_{\text{FB}})V_{tm} - WV_{tm} - XV_{tm}^2 - Y \tag{50}$$

where

$$U = \left(\frac{r_{\text{gear}}}{R_{\text{wheel}}}\right)^2 \frac{90K_{tm}^2}{m(5R_{tm}+5R_{\text{cable}}+R_{fw})} \tag{51}$$

$$W = \frac{B}{m} \tag{52}$$

$$X = C\frac{R_{\text{wheel}}}{3K_{tm}mr_{\text{gear}}} \tag{53}$$

$$Y = \frac{3K_{tm}r_{\text{gear}}A}{mR_{\text{wheel}}} \tag{54}$$

From Eq. (49), the following term must be minimized to maximize the total flywheel energy recovered during the braking E_{fw}. Utilizing Eq. (50) yields

$$\int_0^{t_f}(Mi_{fw} + Ni_{fw}^2 + H + QV_{fw} + RV_{fw}^2)dt = \int_{V_o}^{V_f}\frac{M\frac{1-k_{\text{FB}}}{(5R_{tm}+5R_{\text{cable}}+R_{fw})}V_{tm} + N\left(\frac{(1-k_{\text{FB}})V_{tm}}{5R_{tm}+5R_{\text{cable}}+R_{fw}}\right)^2 + H + Qk_{\text{FB}}V_{tm} + Rk_{\text{FB}}^2V_{tm}^2}{\frac{dV_{tm}}{dt}}dV_{tm}$$
$$= \int_{V_f}^{V_o}\frac{\hat{M}(1-k_{\text{FB}})V_{tm} + \hat{N}(1-k_{\text{FB}})^2V_{tm}^2 + H + Qk_{\text{FB}}V_{tm} + Rk_{\text{FB}}^2V_{tm}^2}{U(1-k_{\text{FB}})V_{tm} + WV_{tm} + XV_{tm}^2 + Y}dV_{tm} \tag{55}$$

where

$$\hat{M} = \frac{M}{(5R_{tm}+5R_c+R_{fw})} \tag{56}$$

$$\hat{N} = \frac{N}{(5R_{tm}+5R_c+R_{fw})^2} \tag{57}$$

Define

$$f(V_{tm}, k_{\text{FB}}) = \frac{\hat{M}(1-k_{\text{FB}})V_{tm} + \hat{N}(1-k_{\text{FB}})^2V_{tm}^2 + H + Qk_{\text{FB}}V_{tm} + Rk_{\text{FB}}^2V_{tm}^2}{U(1-k_{\text{FB}})V_{tm} + WV_{tm} + XV_{tm}^2 + Y} \tag{58}$$

All coefficients of V_{tm} and V_{tm}^2 are positive, and $0 \le V_{tmf} \le V_{tm} \le V_{tmo}$ in Eq. (58); therefore, the integrand of Eq. (55) is positive, and it follows that the integral will be a minimum if the integrand is a minimum for all values of V_{tm} in the range indicated because they can be individually controlled by k_{FB} and only depend on the current V_{tm} value. Treat V_{tm} as a constant in $f(V_{tm}, k_{\text{FB}})$, and set the first derivative to zero (make stationary)

$$\frac{d}{dk_{\text{FB}}}f = \frac{-2\hat{N}V_{tm}^2 + (Q-\hat{M})V_{tm} + 2(R+\hat{N})V_{tm}^2k_{\text{FB}}}{(UV_{tm} + WV_{tm} + XV_{tm}^2 + Y - UV_{tm}k_{\text{FB}})^2}(UV_{tm} + WV_{tm} + XV_{tm}^2 + Y - UV_{tm}k_{\text{FB}})$$
$$+ \frac{\hat{M}UV_{tm}^2(1-k_{\text{FB}}) + \hat{N}UV_{tm}^3(1-k_{\text{FB}})^2 + HUV_{tm} + QUV_{tm}^2k_{\text{FB}} + RUV_{tm}^3k_{\text{FB}}^2}{(UV_{tm} + WV_{tm} + XV_{tm}^2 + Y - UV_{tm}k_{\text{FB}})^2} = 0 \tag{59}$$

or

$$(-2\hat{N}V_{tm}^2 + QV_{tm} - \hat{M}V_{tm})(WV_{tm} + XV_{tm}^2 + Y) - \hat{N}UV_{tm}^3 + HUV_{tm} + QUV_{tm}^2$$
$$+ (2YRV_{tm}^2 + 2Y\hat{N}V_{tm}^2 + 2URV_{tm}^3 + 2WRV_{tm}^3 + 2\hat{N}UV_{tm}^3 + 2W\hat{N}V_{tm}^3 + 2XRV_{tm}^4 + 2X\hat{N}V_{tm}^4)k_{\text{FB}}$$
$$- (R+\hat{N})UV_{tm}^3k_{\text{FB}}^2 = 0 \tag{60}$$

Define

$$C_A = -(R + \hat{N})UV_{tm}^3 \tag{61}$$

$$\begin{aligned} C_B &= 2YRV_{tm}^2 + 2Y\hat{N}V_{tm}^2 + 2URV_{tm}^3 + 2WRV_{tm}^3 + 2\hat{N}UV_{tm}^3 + 2W\hat{N}V_{tm}^3 + 2XRV_{tm}^4 + 2X\hat{N}V_{tm}^4 \\ &= 2Y(R + \hat{N})V_{tm}^2 + 2U(R + \hat{N})V_{tm}^3 + 2W(R + \hat{N})V_{tm}^3 + 2X(R + \hat{N})V_{tm}^4 \end{aligned} \tag{62}$$

$$C_C = (-2\hat{N}V_{tm}^2 + QV_{tm} - \hat{M}V_{tm})(WV_{tm} + XV_{tm}^2 + Y) - \hat{N}UV_{tm}^3 + HUV_{tm} + QUV_{tm}^2 \tag{63}$$

Eq. (60) becomes

$$C_C + C_B k_{\mathrm{FB}} + C_A k_{\mathrm{FB}}^2 = 0 \tag{64}$$

The solution of Eq. (64) will be

$$k_{\mathrm{FB}} = \frac{-C_B \pm \sqrt{C_B^2 - 4C_A C_C}}{2C_A} \tag{65}$$

Observe that

$$\frac{-C_B}{2C_A} = \frac{YV_{tm}^2 + UV_{tm}^3 + WV_{tm}^3 + XV_{tm}^4}{UV_{tm}^3} = 1 + \frac{Y + WV_{tm} + XV_{tm}^2}{UV_{tm}} > 1 \quad \text{and} \quad C_A < 0$$

Therefore, the only root that may fall in the required range $0 \le k_{\mathrm{FB}} \le 1$ is

$$k_{\mathrm{FB}} = \frac{-C_B + \sqrt{C_B^2 - 4C_A C_C}}{2C_A} \tag{66}$$

The k_{FB} value defined in Eq. (66) provides only a necessary condition for the total braking energy to become a minimum. Eq. (66) will also be a sufficient condition if the second derivative of $f\ (V_{tm}, k_{\mathrm{FB}})$ is positive when it is evaluated at the k_{FB} defined in Eq. (66). Taking the second derivative of $f\ (V_{tm}, k_{\mathrm{FB}})$ yields

$$\begin{aligned} \frac{d}{dk_{\mathrm{FB}}}\left(\frac{d}{dk_{\mathrm{FB}}}f\right) &= \frac{d}{dk_{\mathrm{FB}}}\left(\frac{C_C + C_B k_{\mathrm{FB}} + C_A k_{\mathrm{FB}}^2}{(UV_{tm} + WV_{tm} + XV_{tm}^2 + Y - UV_{tm}k_{\mathrm{FB}})^2}\right) \\ &= \frac{C_B + 2C_A k_{\mathrm{FB}}}{(UV_{tm} + WV_{tm} + XV_{tm}^2 + Y - UV_{tm}k_{\mathrm{FB}})^2} + 2\frac{C_C + C_B k_{\mathrm{FB}} + C_A k_{\mathrm{FB}}^2}{(UV_{tm} + WV_{tm} + XV_{tm}^2 + Y - UV_{tm}k_{\mathrm{FB}})^3}UV_{tm} \\ &= \frac{C_B + 2C_A k_{\mathrm{FB}}}{(UV_{tm} + WV_{tm} + XV_{tm}^2 + Y - UV_{tm}k_{\mathrm{FB}})^2} + 2\frac{UV_{tm}}{UV_{tm} + WV_{tm} + XV_{tm}^2 + Y - UV_{tm}k_{\mathrm{FB}}}UV_{tm}\left(\frac{d}{dk_{\mathrm{FB}}}f\right) \end{aligned} \tag{67}$$

Substitute Eq. (66) into Eq. (67), and recall that Eq. (66) produces a zero first derivative of $f(V_{tm}, k_{\mathrm{FB}})$ to obtain

$$\frac{d}{dk_{\mathrm{FB}}}\left(\frac{d}{dk_{\mathrm{FB}}}f\right) = \frac{C_B + 2C_A k_{\mathrm{FB}}}{(UV_{tm} + WV_{tm} + XV_{tm}^2 + Y - UV_{tm}k_{\mathrm{FB}})^2} = \frac{2(R + N\hat{})[YV_{tm}^2 + WV_{tm}^3 + XV_{tm}^4 + UV_{tm}^3(1 - k_{\mathrm{FB}})]}{(UV_{tm} + WV_{tm} + XV_{tm}^2 + Y - UV_{tm}k_{\mathrm{FB}})^2} \tag{68}$$

Case 1: k_{FB} from Eq. (66) satisfies $0 \le k_{\mathrm{FB}} \le 1$. In this case, the right-hand side of Eq. (68) is positive, so that Eq. (66) produces a minimum value of $f(V_{tm}, k_{\mathrm{FB}})$ (maximum value of harvested energy by the flywheel).

Case 2: k_{FB} from Eq. (66) does not satisfy $0 \le k_{\mathrm{FB}} \le 1$. In this case, $f(V_{tm}, k_{\mathrm{FB}})$ varies monotonically within [0, 1] and is minimum at one of the limits $k_{\mathrm{FB}} = 0$ or $k_{\mathrm{FB}} = 1$, which can be determined by substitution.

The k_{FB} value as obtained previously yields the maximum harvested energy obtained from braking the train and is utilized to obtain the required flywheel voltage, per Eq. (22): $V_{fw} = k_{\mathrm{FB}} \times V_{tm}$.

Appendix II. Proof of Monotonicity of Solution

Maximum Regenerative-Braking Energy Recovery Method Solution

Eq. (31) gives the aggregate objective function T to minimize, as follows:

$$\left(\frac{m_{\mathrm{train}}}{F_{\mathrm{brake}}}\right)^2 + b^2\left(\frac{P_{\mathrm{kin\,loss}}}{P_{fw}}\right)^2 = \frac{H}{i_{fw}^2} + \left(\frac{I + Ji_{fw}}{Ki_{fw} - Li_{fw}^2}\right)^2 = \frac{1}{i_{fw}^2}\left[\left(H + \frac{J^2}{L^2}\right) - 2\frac{J}{L}\left(I + \frac{JK}{L}\right)\frac{1}{K - Li_{fw}} + \left(I + \frac{JK}{L}\right)^2\left(\frac{1}{K - Li_{fw}}\right)^2\right] \tag{69}$$

where

$$H = m_{\text{train}}^2 / r_1^2 \tag{70}$$

$$I = b\left(A\frac{R_{\text{wheel}}}{3r_{\text{gear}}K_{tm}}V_{tm} + B\left(\frac{R_{\text{wheel}}}{3r_{\text{gear}}K_{tm}}\right)^2 V_{tm}^2 + C\left(\frac{R_{\text{wheel}}}{3r_{\text{gear}}K_{tm}}\right)^3 V_{tm}^3\right) \tag{71}$$

$$J = 10bV_{tm} \tag{72}$$

$$K = 10V_{tm} \tag{73}$$

$$L = 10(5R_{tm} + 5R_c + R_{fw}) \tag{74}$$

From Eq. (69), define

$$T(i_{fw}) = \frac{1}{i_{fw}^2}\left(\left(H + \frac{J^2}{L^2}\right) - 2\frac{J}{L}\left(I + \frac{JK}{L}\right)\frac{1}{K - Li_{fw}} + \left(I + \frac{JK}{L}\right)^2\left(\frac{1}{K - Li_{fw}}\right)^2\right) \tag{75}$$

The instantaneous flywheel current i_{fw} that minimizes the previously given function T, and the instantaneous traction motor voltage V_{tm} and flywheel angular velocity ω_{fw} are substituted into Eq. (21) to obtain the required flywheel gain value

$$K_{fw} = \frac{1}{\omega_{fw}}[V_{tm} - (5R_{tm} + 5R_{\text{cable}} + R_{fw})i_{fw}] \tag{76}$$

which is physically realized by the flux-weakening approaches described. The function $T(i_{fw})$ in Eq. (75) is minimized with respect to i_{fw}, while treating V_{tm} as a constant at any given time and observing that H, I, J, K, and L are all positive constants. The function $T(i_{fw})$ tends to $+\infty$ as i_{fw} tends to 0 and K/L. From Eq. (21), the corresponding V_{fw} values are $V_{fw} = V_{tm}$ and $V_{fw} = 0$, respectively.

These points confirm that there must be a minimum value of T in the operational range of interest [i.e., $0 < V_{fw} < V_{tm}$ and $0 < i_{fw} < V_{tm}/(5R_{tm} + 5R_{\text{cable}} + R_{fw})$] because T goes to $+\infty$ at both endpoints of interest and $-\infty$ does not exist in this region.

Apply the stationary condition to Eq. (75) with respect to the flywheel current

$$\frac{d}{di_{fw}}\left(\frac{H}{i_{fw}^2} + \left(\frac{I + Ji_{fw}}{Ki_{fw} - Li_{fw}^2}\right)^2\right) = -\frac{2H}{i_{fw}^3} + 2\frac{I + Ji_{fw}}{Ki_{fw} - Li_{fw}^2}\left(\frac{J}{Ki_{fw} - Li_{fw}^2} - \frac{I + Ji_{fw}}{(Ki_{fw} - Li_{fw}^2)^2}(K - 2Li_{fw})\right) = 0 \tag{77}$$

Setting the numerator of this expression to zero yields

$$(HL^3 + J^2L)i_{fw}^3 + (3IJL - 3HKL^2)i_{fw}^2 + (2I^2L - IJK + 3HK^2L)i_{fw} - I^2K - HK^3 = 0 \tag{78}$$

where

$$C_a = (HL^3 + J^2L) \tag{79}$$

$$C_b = (3IJL - 3HKL^2) \tag{80}$$

$$C_c = (2I^2L - IJK + 3HK^2L) \tag{81}$$

$$C_d = -I^2K - HK^3 \tag{82}$$

Then the discriminant of the cubic function in Eq. (78) is

$$\Delta = 18C_aC_bC_cC_d - 4C_b^3C_d + C_b^2C_c^2 - 4C_aC_c^3 - 27C_a^2C_d^2 \tag{83}$$

If $\Delta \le 0$, Eq. (78) will have only one real root as expressed in Eq. (84)

$$i_{fw} = -\frac{C_b}{3C_a} - \frac{1}{3C_a}\sqrt[3]{\frac{1}{2}[2C_b^3 - 9C_aC_bC_c + 27C_a^2C_d + \sqrt{(2C_b^3 - 9C_aC_bC_c + 27C_a^2C_d)^2 - 4(C_b^2 - 3C_aC_c)^3}]}$$
$$-\frac{1}{3C_a}\sqrt[3]{\frac{1}{2}[2C_b^3 - 9C_aC_bC_c + 27C_a^2C_d - \sqrt{(2C_b^3 - 9C_aC_bC_c + 27C_a^2C_d)^2 - 4(C_b^2 - 3C_aC_c)^3}]} \tag{84}$$

As discussed previously, there must be at least one minimum within the practical range of interest $i_{fw} \in [0, V_{tm}/(5R_{tm} + 5R_c + R_{fw})]$, and Eq. (84) is the only possible minimum position solution. It can be concluded that Eq. (84) is the optimum solution if $\Delta \le 0$, which is the case observed during simulations.

When $\Delta > 0$, there will be three distinct real roots for Eq. (78).

One of the roots is given by Eq. (84), and the other two roots are as listed in Eq. (85) and Eq. (86)

$$i_{fw\_2} = -\frac{C_b}{3C_a} + \frac{1+i\sqrt{3}}{6C_a}\sqrt[3]{\frac{1}{2}[2C_b^3 - 9C_aC_bC_c + 27C_a^2C_d + \sqrt{(2C_b^3 - 9C_aC_bC_c + 27C_a^2C_d)^2 - 4(C_b^2 - 3C_aC_c)^3}]} + \frac{(1-i\sqrt{3})(C_b^2 - 3C_aC_c)}{6C_a\sqrt[3]{\frac{1}{2}[2C_b^3 - 9C_aC_bC_c + 27C_a^2C_d + \sqrt{(2C_b^3 - 9C_aC_bC_c + 27C_a^2C_d)^2 - 4(C_b^2 - 3C_aC_c)^3}]}} \tag{85}$$

$$i_{fw\_3} = -\frac{C_b}{3C_a} + \frac{1-i\sqrt{3}}{6C_a}\sqrt[3]{\frac{1}{2}[2C_b^3 - 9C_aC_bC_c + 27C_a^2C_d + \sqrt{(2C_b^3 - 9C_aC_bC_c + 27C_a^2C_d)^2 - 4(C_b^2 - 3C_aC_c)^3}]} + \frac{(1+i\sqrt{3})(C_b^2 - 3C_aC_c)}{6C_a\sqrt[3]{\frac{1}{2}[2C_b^3 - 9C_aC_bC_c + 27C_a^2C_d + \sqrt{(2C_b^3 - 9C_aC_bC_c + 27C_a^2C_d)^2 - 4(C_b^2 - 3C_aC_c)^3}]}} \tag{86}$$

As discussed previously, for the $\Delta > 0$ case, at least one of the three real roots must fall in the range $0 < V_{fw} < V_{tm}$ and $0 < i_{fw} < V_{tm}/(5R_{tm} + 5R_c + R_{fw})]$. The procedure will be to evaluate $T(i_{fw})$ at each root and then utilize the i_{fw} that produces the smallest $T(i_{fw})$, in the following formula [Eq. (76)]:

$$K_{fw} = \frac{1}{\omega_{fw}}[V_{tm} - (5R_{tm} + 5R_{\text{cable}} + R_{fw})i_{fw}]$$

As is shown, the only poles of the rational function $T(i_{fw})$ occur at the endpoints of the range of all possible values of i_{fw}, which corresponds to flywheel voltages equal to 0 and V_{tm}. The first value only occurs if the train is stopped, and the second condition can never occur because of resistive voltage drops in the circuit.

Proof of Monotonicity of Solution

This section demonstrates that

a. The energy recovery efficiency $[P_{fw}/(P_{\text{Davis}} - P_{tm})]$ increases monotonically with increasing b, and
b. The braking effort (traction motor forced acceleration = F_{tm}/m_{train}) decreases monotonically with increasing b.

Assume

$$Q_1(i_{fw}) = \frac{m_{\text{train}}}{F_{tm}} \tag{87}$$

$$Q_2(i_{fw}) = \frac{P_{\text{Kin Loss}}}{P_{fw}} \tag{88}$$

The minimization target function becomes

$$T(i_{fw}) = (Q_1(i_{fw}))^2 + b^2(Q_2(i_{fw}))^2 \tag{89}$$

Assume that i_{fw1} and i_{fw2} are minimum solutions within the range $[0, V_{tm}/(5R_{\text{tm}} + 5R_c + R_{\text{fw}})]$ for Eq. (89) at b_1 and b_2 $(b_1 > b_2)$. Because for a fixed i_{fw} value $Q_1(i_{fw})$ and $Q_2(i_{fw})$ are also fixed, it can be assumed that

$$\begin{cases} Q_{11} = Q_1(i_{fw1}) \\ Q_{21} = Q_2(i_{fw1}) \end{cases} \tag{90}$$

$$\begin{cases} Q_{12} = Q_1(i_{fw2}) \\ Q_{22} = Q_2(i_{fw2}) \end{cases} \tag{91}$$

Because i_{fw1} is the minimum solution at b_1 and i_{fw2} is the minimum solution at b_2, the following is derived:

$$Q_{11}^2 + b_1^2Q_{21}^2 < Q_{12}^2 + b_1^2Q_{22}^2 \tag{92}$$

$$Q_{12}^2 + b_2^2Q_{22}^2 < Q_{11}^2 + b_2^2Q_{21}^2 \tag{93}$$

a. By adding Eq. (92) and Eq. (93), the following is derived:

$$b_1^2Q_{21}^2 + b_2^2Q_{22}^2 < b_1^2Q_{22}^2 + b_2^2Q_{21}^2 \tag{94}$$

which converts to

$$(b_1^2 - b_2^2)Q_{21}^2 < (b_1^2 - b_2^2)Q_{22}^2 \tag{95}$$

Because $(b_1^2 - b_2^2) > 0$, the following is derived:

$$Q_{21}^2 < Q_{22}^2 \tag{96}$$

Because $Q_2(i_{fw}) > 0$

$$Q_{21} < Q_{22} \tag{97}$$

By definition of Eq. (88), this indicates that for a higher b value (b_1), the energy recovery efficiency is greater.

b. By dividing Eq. (92) with b_1^2, dividing Eq. (93) with b_2^2, and adding the results together, the following is derived:

$$\frac{Q_{11}^2}{b_1^2} + \frac{Q_{12}^2}{b_2^2} < \frac{Q_{12}^2}{b_1^2} + \frac{Q_{11}^2}{b_2^2} \tag{98}$$

which converts to

$$(b_1^2 - b_2^2)Q_{12}^2 < (b_1^2 - b_2^2)Q_{11}^2 \tag{99}$$

Because $(b_1^2 - b_2^2) > 0$ and $Q_1(i_{fw}) > 0$

$$Q_{12} < Q_{11} \tag{100}$$

By definition of Eq. (87), this indicates that for a higher b value (b_1), the braking effort is smaller because it is the inverse of Q_1.

Acknowledgments

The authors wish to express their gratitude to the Association of American Railroads (AAR) for funding this research and for the valuable comments of Professor Gary Fry (Texas A&M AAR

Center Director) and Mike Iden (General Director, Car and Locomotive Engineering, Union Pacific Railroad).

References

AiResearch Manufacturing Company of California. (1979). "Flywheel energy storage switcher. Volume I. Study summary and detailed description of analysis." *Prepared for U.S. Dept. of Transportation and Federal Railroad Administration*, *Rep. No. FRA/ORD-79/20.1*, Torrance, CA.

Brockbank, C., and Greenwood, C. (2009). "Fuel economy benefits of a flywheel & CVT based mechanical hybrid for city bus and commercial vehicle applications." *SAE 2009 Commercial Vehicle Engineering Congress & Exhibition*, Society of Automotive Engineers, Warrendale, PA.

Caprio, M. T., Murphy, B. T., and Herbst, J. D. (2004). "Spin commissioning and drop tests of a 130 kW-hr composite flywheel." *Proc., 9th Int. Symp. on Magnetic Bearings*, Technomic Publishing, Lancaster, PA.

Deb, K. (2001). *Multi-objective optimization using evolutionary algorithms*, Wiley, New York.

Deb, K., Pratap, A., Agarwal, S., and Meyarivan, T. (2002). "A fast and elitist multi-objective genetic algorithm: NSGA-II." *IEEE Trans. Evol. Comput.*, 6(2), 182–197.

El-Refaie, A. M., Novotny, D. W., and Jahns, T. M. (2004). "A simple model for flux weakening in surface PM synchronous machines using back-to-back thyristors." *IEEE Power Electron. Lett.*, 2(2), 54–57.

Fritz, S. G. (2000). "Diesel fuel effects on locomotive exhaust emissions." *Rep. Prepared for California Air Resources Board*, Southwest Research Institute, San Antonio, TX.

Hawkins, L., Murphy, B., Zierer, J., and Hayes, R. (2003). "Shock and vibration testing of an AMB supported energy storage flywheel." *JSME Int. J. Ser. C*, 46(2), 429–435.

Huang, Y. M., and Wang, K. J. (2007). "A hybrid power driving system with an energy storage flywheel for vehicles." *SAE 2007 commercial vehicle engineering congress & exhibition*, Society of Automotive Engineers, Warrendale, PA.

Kenny, B., Kascak, P., Jansen, R., Dever, T., and Santiago, W. (2005). "Control of a high-speed flywheel system for energy storage in space applications." *IEEE Trans. Ind. Appl.*, 41(4), 1029–1038.

Maschinenfabrik Oerlikon of Switzerland. (1958). "N.C.B. electrogyro locomotive." *Railway Mag.*, 421.

Park, J., Palazzolo, A., and Beach, R. (2008). "MIMO active vibration control of magnetically suspended flywheels for satellite IPAC service." *J. Dyn. Syst. Meas. Control*, 130(4), 041005.

Sierra Research Inc. (2004). "Development of railroad emissions inventory technologies." *Prepared for the Southeastern States Air Resources Managers Inc.*, *Rep. No. 2004-06-02*, Sacramento, CA.

Thelen, R. F., Herbst, J. D., and Caprio, M. D. (2003). "A 2 MW flywheel for hybrid locomotive power." *Proc., IEEE Vehicular Technology Conf. (VTC2003-Fall)*, IEEE, New York, 6, 3231–3235.

U.S. Energy Information Administration (EIA). (2010). *Annual energy review 2009*, Washington, DC.

U.S. Environmental Protection Agency (EPA). (1998). "Emission standards for locomotives and locomotive engines: Final rule." *Federal Register, 63* (No. 73; April 16), 18978.

U.S. Environmental Protection Agency (EPA). (2005). "Emission facts, EPA420-F-05-001." ⟨http://www.epa.gov/otaq/climate/420f05001.pdf⟩ (Nov. 1, 2010).

U.S. Environmental Protection Agency (EPA). (2010). "eGRID2010 year 2007 plant and aggregation files and file structure." ⟨http://www.epa.gov/cleanenergy/energy-resources/egrid/index.html⟩ (Nov. 1, 2010).

William, W. H. (1982). *Railroad engineering*, 2nd Ed., Wiley, New York.

Wilson, B. C. D., and Fausz, J. L. (2006). "Secondary energy storage trade space analysis for high peak power applications." *Proc., 2006 Space Power Workshop*, April 25–27, 2006, Manhattan Beach, CA.